RIGA TECHNICAL UNIVERSITY

Deniss Kolosovs

ADAPTIVE BLIND EQUALIZATION ALGORITHMS FOR QAM SYSTEMS

Summary of the Doctoral Thesis

RTU Press
Riga 2022

RIGA TECHNICAL UNIVERSITY

Faculty of Electronics and Telecommunications

Institute of Radioelectronics

Deniss Kolosovs

Doctoral Student of Study Programme “Electronics”

ADAPTIVE BLIND EQUALIZATION ALGORITHMS FOR QAM SYSTEMS

Summary of the Doctoral Thesis

Scientific supervisors:

Associate Professor Dr. sc. ing.
ARTŪRS ĀBOLTIŅŠ

Associate Professor Dr. sc. ing.
ANNA LITVIŅENKO

RTU Press

RIGA 2022

Kolosovs D. Adaptive Blind Equalization Algorithms for QAM Systems. Summary of the Doctoral Thesis. — Riga: RTU Press, 2022. — 49 p.

Published in accordance with the decision of the Promotion Council "RTU P-08" of 4 March 2022, Minutes No. 8.

The research was partially performed within the framework and with financial support of the SAM 8.2.2. "Stiprināt augstākās izglītības institūciju akadēmisko personālu stratēģiskās specializācijas jomās" project of Riga Technical University No. 8.2.2.0/18/A/017.

https://doi.org/10.7250/9789934227882
ISBN 978-9934-22-788-2 (pdf)

DOCTORAL THESIS PROPOSED TO RIGA TECHNICAL UNIVERSITY FOR THE PROMOTION TO THE SCIENTIFIC DEGREE OF DOCTOR OF SCIENCE

To be granted the scientific degree of Doctor of Science (Ph. D.), the present Doctoral Thesis has been submitted for the defence at the open meeting of RTU Promotion Council on 10 June 2022, 13:30, at the Faculty of Electronics and Telecommunications of Riga Technical University, 12 Āzenes Street, Room 201.

OFFICIAL REVIEWERS

Professor, Dr. sc. ing. Vjačeslavs Bobrovs
Riga Technical University

Professor, Dr.-Ing. habil. Andreas Ahrens
Hochschule Wismar, University of Applied Sciences Technology, Business and Design, Germany

Associate Professor, Dr. Rasa Brūzgienė
Kaunas University of Technology, Lithuania

DECLARATION OF ACADEMIC INTEGRITY

I hereby declare that the Doctoral Thesis submitted for the review to Riga Technical University for the promotion to the scientific degree of Doctor of Science (Ph. D.) is my own. I confirm that this Doctoral Thesis had not been submitted to any other university for the promotion to a scientific degree.

Deniss Kolosovs _____

Date: _____

The Doctoral Thesis has been written in English. It consists of Introduction, 5 chapters, Conclusions, 35 figures, 3 tables, 4 appendices; the total number of pages is 98, not including appendices. The Bibliography contains 80 titles.

CONTENTS

ACRONYMS 6
INTRODUCTION 7
Rationale 7
The Purpose Statement and the Objectives 7
The Subject and the Object of the Research 8
Research methodology 8
Scientific Novelty and Main Results 9
The Theses to be Defended 9
The Approbation and Practical Significance 10
The Structure of the Thesis 12
1 GENERAL DESCRIPTION OF THE RESEARCH FIELD 13
1.1 Quadrature Amplitude Modulation Concept 13
1.2 Complex Baseband Model of the QAM Communication System 15
1.3 Complex Baseband Multipath Channel Model 18
1.4 Equalization of QAM Signals 20
1.5 Blind Equalization Concept 20
1.6 Conclusions 21
2 ENHANCED DECISION-ADJUSTED MODULUS ALGORITHM 22
2.1 Decision-Adjusted Multimodulus Algorithm 22
2.2 Error Statistical Properties 22
2.3 Enhanced DAMA 24
2.4 Simulation Results 25
2.5 Conclusions 27
3 GROUPED RADII APPROACH 28
3.1 An Impact of Detection Error Probability on the Convergence of Equalizer . 28
3.2 Detection Error Probability as a Function of Output Radius Variance 28
3.3 Proposed Optimization Procedure 29
3.4 Simulation results 31
3.5 Conclusions 33
4 ADAPTIVE SWITCHED GR-DAMA APPROACH 35
4.1 Error Measurement Methods 35
4.2 Simulation Results 36
4.3 Conclusions 38
5 FPGA IMPLEMENTATION AND FIELD MEASUREMENTS 39
5.1 Design Objectives 39
5.2 Fixed-Point Arithmetic Implementation 39

5.3 Blind Equalizer Implementation 40
5.4 FPGA Test Environment Implementation 40
5.5 Implementation Results 41
5.6 Conclusions 42
FINAL CONCLUSIONS 44
BIBLIOGRAPHY 45

ACRONYMS

ACF autocorrelation function

ACM adaptive coding and modulation

ADC analog-to-digital converter

AWGN additive white Gaussian noise

CMA constant modulus algorithm

DAC digital-to-analog converter

DAMA decision adjusted modulus algorithm

EDAMA enhanced decision-adjusted modulus algorithm

ETSI European Telecommunications Standards Institute

FCC Federal Communications Commission

FPGA field-programmable gate array

IP intellectual property

ISI inter-symbol interference

MIMO multiple-input and multiple-output

OFDM orthogonal frequency-division multiplexing

PAPR peak-to-average power ratio

PDF probability density function

PDM polarization-division multiplexing

PSAM pilot symbol assisted modulation

QAM quadrature amplitude modulation

VHDL VHSIC hardware description language

VHSIC very high speed integrated circuit

WSSUS wide-sense stationary uncorrelated scattering

XPIC cross-polarization interference canceling

INTRODUCTION

Rationale

Quadrature amplitude modulation (QAM) is a common signal forming method in modern wireless data transmission systems. Moreover, the QAM approach underlies many communication technologies, e.g., orthogonal frequency-division multiplexing (OFDM), multiple-input and multiple-output (MIMO), and polarization-division multiplexing (PDM). This work considers mitigation of multipath phenomenon—QAM signal propagation effect that significantly degrades receiving quality if not handled. Usually, compensation is performed with the help of an equalizer, a filter with adjustable coefficients.

Techniques such as training sequence transmission, low order modulation usage, adaptive coding and modulation (ACM) involvement in the acquisition process, and predefined symbols interleaving with user traffic (in pilot symbol assisted modulation (PSAM)) are typically used to adjust the equalizer. However, these methods either require a service channel and full-duplex link or reduce capacity.

Blind adjustment is an alternative solution to the problem. It does not require predefined symbol transmission and thus does not have the drawbacks of the methods described above. The most common algorithm of this group of equalization approaches, constant modulus algorithm (CMA), was laid down in [1], [2]. It is characterized by good convergence properties but a high residual error level. There are groups of publications that aim to eliminate this shortcoming: using multiple dispersion constants [3], [4], processing the received symbol's real and imaginary parts separately [5]–[7], applying multiple-mode algorithms [8]–[15], or joining several approaches [16], [17].

Extensions to blind alignment algorithms are used to minimize the peak-to-average power ratio (PAPR) problem and recover carrier in OFDM [18]–[20], suppressing inter-source interference in MIMO [21]–[23], cross-polarization interference canceling (XPIC) [24]–[26], beam separations in phased antenna arrays in massive MIMO [27]–[31], and joint equalization and timing or carrier recovery [32], [33].

Although there are many blind equalization algorithms, their limitations make them an optimal signal processing tool only in particular operating requirements. The field of blind alignment requires an approach to form an algorithm suitable for given working conditions. A generalized CMA-like algorithm, which is the purpose of this Doctoral Thesis, might also be applied in the cases described above.

The Objective Statement and the Tasks

The **objective** of this Doctoral Thesis is the generalization of existing CMA-like algorithms and the development of a blind equalization technique that will ensure performance for the defined operating

conditions. The following **tasks** are stated to achieve the previously defined objectives:

- Description of the utilized multipath channel and QAM-based communication system.
- Exploration of popular blind equalization algorithms with the fixation of their drawbacks.
- Suggestion of a new algorithm to minimize misadjustment probability.
- Generalization of the proposed algorithm to ensure its operation in dual and multiple modes.
- Establishment of the "Stop-and-Go" concept for switching between modes.
- Field-programmable gate array (FPGA) implementation of the equalizer tuned by the proposed algorithm and its incorporation into QAM modem and field measurements.

The Subject and the Object of the Research

The **object** of this research is a baseband of a QAM communication system. Regarding our research, it consists of signal forming part, baseband model of a multipath channel with additive white Gaussian noise (AWGN), and QAM receiver (contains matched filter, a gain control system, and timing recovery, equalization system, and the received symbol estimating block).

The **subject** of this research is the blind equalization algorithm. The purpose of this mechanism is an adjustment of the equalizer taps. Typically, it is a structure that performs analysis of current equalizer output, estimates the algorithm cost function, and evaluates the current vector of increments for equalizer taps coefficients.

Research Methodology

The current Doctoral Thesis adapts several engineering projects; thus, the research methodology is conditioned by a set of technical tasks. The following incremental steps have made development from the initial idea to the final algorithm:

- Exploration of existing solutions limits and drawbacks.
- Specification of terms of reference for a developing method.
- Formulation of an idea whose implementation can fulfill the terms.
- Analytical exploration of the idea and confirmation of its productivity.
- Implementation in script language for rapid prototyping (Matlab or Python) and simulation.
- Numerical Monte Carlo verification of the convergence properties and residual error levels.
- Implementation in a hardware description language (VHDL) and solution incorporation into the existing scheme.
- Field experiments and verification, whether the proposed method is consistent and meets the requirements.

Scientific Novelty and Main Results

Original ideas that form the overall scientific contribution provided by this research appeared in separate publications and are described for the first time in the body of this document:

- The minimization of detection error probability was used to optimize the cost function of a blind equalization algorithm.
- A cost function, which is dependent on the residual level of inter-symbol interference (ISI) at the output of the equalizer, is utilized in an algorithm of blind equalization.
- The grouping of constellation points in the cost function of the blind equalization algorithm is used for the definition of initial limit values of ISI.
- Grouping constellation points in the cost function of a blind equalization algorithm is used to minimize misadjustment probability in the case of high order modulation and high interference level.
- The stop-and-go algorithm is used to switch to a smoother equalization algorithm.

The list below outlines the main practical results of this research:

- A probability-based enhancement for decision adjusted modulus algorithm (DAMA) that significantly increases its acquisition ability and convergence speed has been proposed.
- An algorithm for blind adjustment of the equalizer that guarantees the maximum limiting probability of detection error for a given initial ISI has been proposed.
- A multiple-mode blind equalization algorithm with a parametric constellation-based cost function is proposed.
- An approach to synthesizing blind alignment algorithms that satisfy the receiving conditions is proposed.

The Theses to be Defended

1. Applying of the enhanced decision-adjusted modulus algorithm instead of the constant modulus algorithm for the blind equalization of a QAM signal ensures zero-dispersion residual error in the case of equalizer impulse response adjusted so that its convolution with the channel impulse response produces delta-function.
2. The usage of optimal symbol detection thresholds in the enhanced decision adjusted modulus algorithm (DAMA) allows decreasing the number of the equalizer coefficients misadjustment events compared to the ordinary DAMA algorithm.
3. Grouping the QAM constellation points in the case of inter-symbol interference (ISI) induced signal dispersion equal to or higher than signal dispersion without ISI allows decreasing the number of the equalizer coefficients misadjustment events and thus increases equalizer convergence probability.
4. The gradual switching of the QAM constellation point grouping algorithms introduces the up-

per limit of the detection error probability in the blind decision-directed equalizer coefficients adjustment.

The Approbation and Practical Significance

The equalizer as an intellectual property (IP) core has been implemented in VHSIC hardware description language (VHDL) and afterwards incorporated in a working QAM modem in FPGA. Field measurements have been performed, as well as modem and equalizer compliance with European Telecommunications Standards Institute (ETSI) and Federal Communications Commission (FCC) standards has been tested with a positive result. Latvian JSC "SAF Tehnika" has experience in the serial production of this device. When writing this Thesis, devices using the proposed blind equalization technique are deployed in the US, the EU, and some Asian countries and provide microwave links.

The following list enumerates publications that reflect the most important ideas of this Thesis (three less significant publications are listed in the Bibliography [34]–[36]):

[37] S. Šarkovskis et al. "Encoder Improvement for Simple Amplitude Fully Parallel Classifiers Based on Grey Codes." In: *Procedia Engineering* 178 (2017), pp. 604–614. ISSN: 18777058. DOI: 10.1016/j.proeng.2017.01.119

[38] D. Kolosovs, A. Zelenkov, and A. Jersovs. "Enhanced Decision Adjusted Modulus Algorithm for Blind Equalization." In: *Procedia Computer Science* 104 (2017), pp. 429–436. ISSN: 18770509. DOI: 10.1016/j.procs.2017.01.156

[39] D. Kolosovs. "A Generalization of the Enhanced Decision Adjusted Modulus Algorithm for Blind Equalization of Constellations with Closely Positioned Circles." In: *2020 IEEE Microwave Theory and Techniques in Wireless Communications (MTTW) (MTTW'20)*. Riga, Latvia: IEEE, Oct. 2020, pp. 195–200. ISBN: 978-1-72819-398-4. DOI: 10.1109/MTTW51045.2020.9244924

[40] D. Kolosovs. "A Multi-Mode Approach for the Enhanced Decision Adjusted Modulus Algorithm Usage in Blind Equalization of QAM Signals." In: *2021 IEEE Microwave Theory and Techniques in Wireless Communications (MTTW)*. Riga, Latvia: IEEE, Oct. 2021, pp. 40–45. ISBN: 978-1-66542-469-1. DOI: 10.1109/MTTW53539.2021.9607265

The author presented the ideas reflected in this Doctoral Thesis at the following international scientific conferences:

1. D. Kolosovs. Chaos code division multiplexing communication system. 7th International Conference on Computational Intelligence, Communication Systems and Networks, 3–5 June 2015, Riga.
2. D. Kolosovs. Equalization possibilities for Non-harmonic Multicarrier communication systems. Riga Technical University 56th International Scientific Conference, Section Electronics,

14–16 October 2015, Riga.

3. D. Kolosovs. A generalization of the enhanced decision adjusted modulus algorithm for blind equalization of constellations with closely positioned circles. 2020 IEEE Microwave Theory and Techniques in Wireless Communications (MTTW), 1–2 October 2020, Riga.
4. D. Kolosovs. A Multi-Mode Approach for the Enhanced Decision Adjusted Modulus Algorithm Usage in Blind Equalization of QAM Signals. 2021 IEEE Microwave Theory and Techniques in Wireless Communications (MTTW), 7–8 October 2021, Riga.

During the writing of the dissertation, the author participated in a number of projects. The list below enumerates the projects in which some of the ideas described in the paper were implemented or the study results were used.

1. Research No. 1.20. "Integra—New Generation Data Transmission Solutions" of the "Latvian Electrical and Optical Equipment Industry Competence Center."
2. Research No. 1.19. "Experimental Development for Data Transmission in Radio Frequency Bands above 60 GHz" of the "Latvian Electrical and Optical Equipment Industry Competence Center."
3. Research No. 1 "Wideband Dual Polarization Radio" of the "Latvian Electrical and Optical Equipment Industry Competence Center." Project 1.2.1.1./16/A/002.
4. SAM 8.2.2. "Rīgas Tehniskās universitātes akadēmiskā personāla stiprināšana stratēģiskās specializācijas jomās," in Riga Technical University. Project 8.2.2.0/18/A/017.
5. Research "Real-Time Spectrum Analyzer Structure and Material Research " of the "Latvian Electrical and Optical Equipment Industry Competence Center." Project 1.2.1.1/18/A/006.

The following courses at Riga Technical University have been developed using the results of this Doctoral Thesis:

1. RRI705 "5G Wireless Technologies," 4.5 ECTS credits.
2. RRI706 "5G Wireless Technologies (course project)," 3.0 ECTS credits.
3. RTR532 "Simulation of Functional and Logical Circuits," 6.0 ECTS credits.
4. RRI324 "Digital Signal Processing," 3.0 ECTS credits.

The multiple modes parametric blind equalization algorithm presented in the Thesis generalizes CMA. It ensures the same or better equalizer convergence and has a zero steady-state and high tracking stability in case of successful convergence. The algorithm proved its properties in test stands and showed an end-user stable operation in the exploitation process. Therefore, a replacement of CMA by this algorithm has no drawbacks except a slight increase in implementation complexity, which is not a crucial problem for modern chips.

The Structure of the Thesis

The Thesis contains five chapters describing development and verification of the proposed approach. Chapter 1 is devoted to the basics of the QAM communication system and the models of baseband multipath channels. Chapter 2 is dedicated to the probabilistic approach to enhancing the target function of DAMA. Chapter 3 introduces an approach to the grouping of constellation points. Chapter 4 proposes a multiple mode parametric algorithm of blind equalization and studies various cost function switching approaches in a multi-mode algorithm. Chapter 5 describes a VHDL implementation of the equalizer based on the proposed algorithm. It also contains the data on the equalizer connection to the QAM modem and the testing of the FPGA prototype.

1 GENERAL DESCRIPTION OF THE RESEARCH FIELD

1.1 Quadrature Amplitude Modulation Concept

The modulation process in data transmission systems ensures the transfer of the spectral density of a band-limited signal from zero to the carrier frequency region. In this way, it is possible to solve the following tasks:

- to provide frequency division of channels or users;
- to form a signal suitable for transmission and reception in wireless data transmission systems (to ensure that the resonance frequency of the antenna and the center frequency of the modulated signal correspond).

The QAM approach can be considered a signal modulation method that eliminates the disadvantage of a twofold reduction in spectral efficiency. It uses the orthogonality property of sine and cosine functions of the same frequency f_0. In this case, two arbitrary signals $s_{\mathrm{I}}(t)$ and $s_{\mathrm{Q}}(t)$, which we will call the quadrature components, modulate carriers $\cos 2\pi f_0 t$ and $-\sin 2\pi f_0 t$, respectively. Thus, the signal obtained using this method can be expressed as

$$s_{\mathrm{QAM}}(t) = s_{\mathrm{I}}(t)\cos 2\pi f_0 t - s_{\mathrm{Q}}(t)\sin 2\pi f_0 t. \tag{1.1}$$

A QAM transmitter requires a digital-to-analog converter (DAC). In the analog signal at the output of this device, copies of the spectral density of the signal remain at frequencies that are multiples of the sampling frequency F_s. However, it must be noted that depending on the type of interpolation used in the DAC, these images may be partially suppressed. Nevertheless, the presence of a DAC implies the setting of a smoothing filter to suppress unnecessary spectral components in the analog signal. The QAM transmitter block diagram is shown in Fig. 1.1.

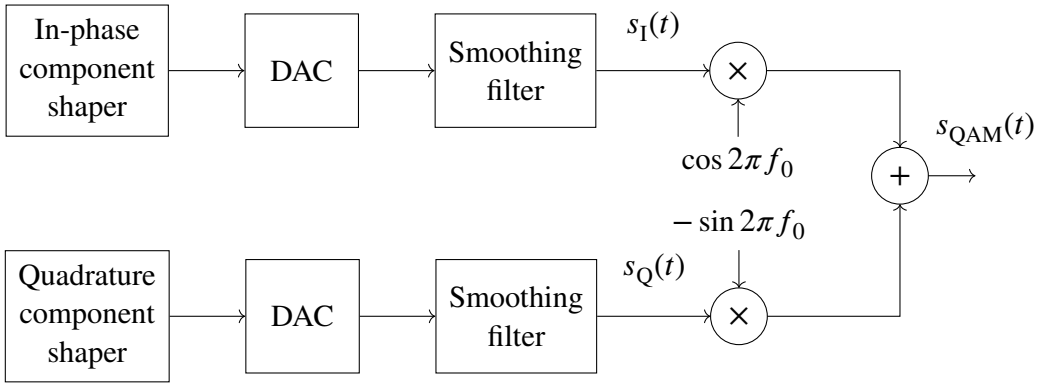

Fig. 1.1. QAM transmitter block diagram

The recovery of the transmitted data at the receiver requires demodulation of signal $s_{\mathrm{QAM}}(t)$. Given the narrowband requirement for modulating signals $\Delta f \ll f_0$, it can be assumed constant

for several carrier periods. Thus, according to orthogonality definition, it is necessary to multiply the received signal and the carrier and integrate the product over time to estimate the correlation in a certain period. The demodulation result can be expressed in the following way:

$$\hat{s}_{\mathrm{I}}(t): \quad s_{\mathrm{QAM}}(t)\cos 2\pi f_0 t = \frac{s_{\mathrm{I}}(t)}{2} + \frac{s_{\mathrm{I}}(t)}{2}\cos 4\pi f_0 t - \frac{s_{\mathrm{Q}}(t)}{2}\sin 4\pi f_0 t; \tag{1.2}$$

$$\hat{s}_{\mathrm{Q}}(t): \quad s_{\mathrm{QAM}}(t)\cos 2\pi f_0 t = \frac{s_{\mathrm{Q}}(t)}{2} - \frac{s_{\mathrm{I}}(t)}{2}\cos 4\pi f_0 t - \frac{s_{\mathrm{Q}}(t)}{2}\sin 4\pi f_0 t. \tag{1.3}$$

Within the framework of this research, the forming, processing, and detection take place on discrete signals. Therefore, a necessary part of the receiver is an analog-to-digital converter (ADC). Obviously, to fulfill the Sampling theorem and avoid overlapping the spectral densities of the signal after sampling, it is necessary to suppress the spectral components above the Nyquist frequency $f_{\mathrm{N}} = 0.5 f_{\mathrm{s}}$, where f_s is the ADC clock frequency. Thus, an anti-aliasing filter must be placed before the ADC. It is a low-pass filter with a cutoff frequency equal to the Nyquist frequency f_{N}. Since the anti-aliasing filter is more stringent than the aforementioned integrating filter (for narrowband signals), the two blocks are usually combined. The structure of the QAM receiver that performs the above actions is shown in Fig. 1.2.

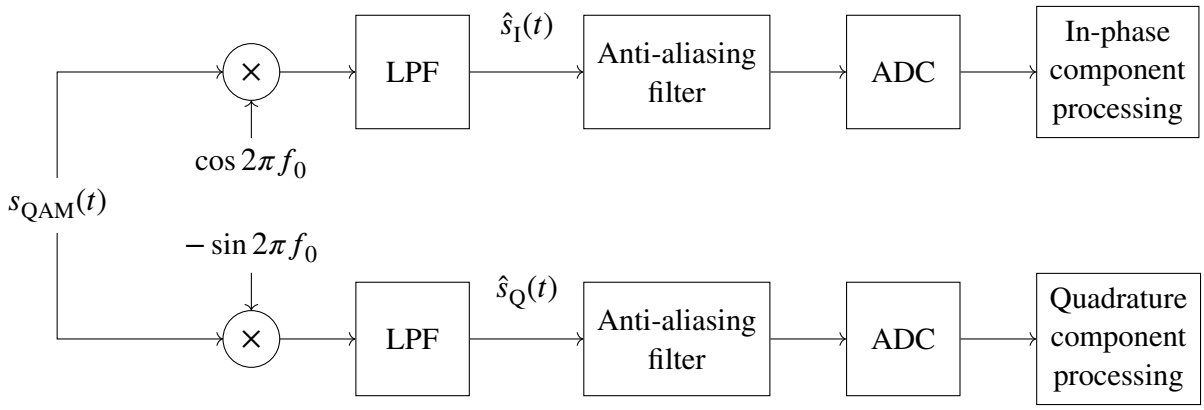

Fig. 1.2. QAM receiver block diagram

The most straightforward data transmission system consists of three parts: a transmitter, which generates a signal intended for transmission; a propagation channel, which is a medium for signal transmission; and a receiver, which extracts information from the transmitted signal. A structural diagram of such a data transmission system is shown in Fig. 1.3.

In Fig. 1.3, the block in which AWGN $n(t)$ is applied to the transmitted signal is shown separately from the channel. That approach is made for two reasons. First, in wireless data transmission systems, the primary source of such noise is the first stages of the radio path of the receiver, especially the low-noise radio frequency amplifier. Secondly, due to the specifics of this work, the channel is singled out separately as a model for effects added by the multipath propagation.

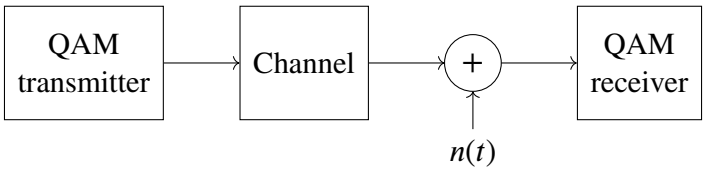

Fig. 1.3. Block diagram of QAM wireless data transmission system

1.2 Complex Baseband Model of the QAM Communication System

Fig. 1.4 shows the complex baseband model of the QAM-based communication system used.

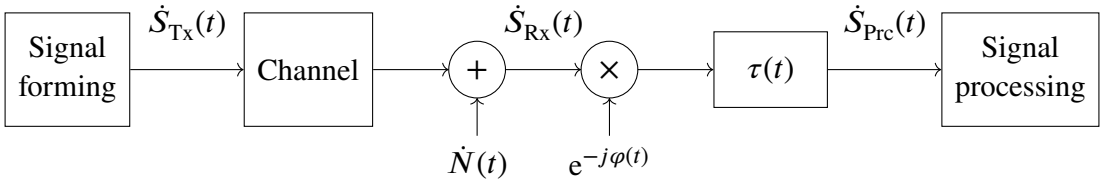

Fig. 1.4. Complex baseband model of the QAM-based wireless data transmission system

The model takes into account the band limitation and discreteness of the processed signals. The model can be used to describe the communication system shown in Fig. 1.3 if the following conditions are met:

1. The smoothing filter is present in the system, and its attenuation in the stopband is sufficient to ignore the suppressed spectral components corresponding to the harmonics of the sampling frequency F_s.
2. The modulating signal bandwidth to the carrier frequency ratio is such $\Delta f \ll f_0$ that the signal can be considered a narrowband.
3. The changes in the channel parameters over time are slow enough to be considered time-invariant for several carrier periods.
4. The difference in carrier frequencies at the transmitter and receiver (mean value of the $\varphi(t)$ time derivative) is that passing the demodulated signal through the low-pass filter and anti-aliasing filter does not introduce linear distortion into the signal.
5. The anti-aliasing filter is present in the system. Its stopband attenuation is sufficient to ignore the spectral components corresponding to frequencies above half the sample rate. The same requirement has been put forward to attenuate the spectral components of the sum of the transmitter and the receiver carrier frequencies.
6. The sampling frequency must be chosen so that the Sampling theorem is fulfilled for each quadrature channel. Additionally, it must be possible to implement smoothing filters after the DAC.

7. Suppose the sampling rate at the receiver is greater than the sampling rate at the transmitter. In that case, the expansion of the spectral density of the signal should not lead to linear distortions in the digital filtering structures of the receiver.

In the complex baseband model of the QAM data transmission system shown in Fig. 1.4, the node that implements signal shaping on the transmitter is designated as a "Signal forming" block. It performs the following operations:

- generates user data, which is a sequence of integers $\{m_k | 0 \leqslant m_k < M\}$, where m_k is kth generated integer, an amount of user data, and $M \in \mathbb{N}$ is the cardinality of the set from which these integers are taken; all elements of the set are equally probable, and the autocorrelation function of a given sequence is a delta-function;
- maps of a piece of user information corresponding to a sequence element m_k to the instantaneous values of the transmitted signal a_k (taken from the set $\{a_k\}$);
- inserts zeros between signal values corresponding to symbols a_k at times $t = kT_{\text{sym}}$, where k is an integer, T_{sym} is a symbol length;
- passes the formed signal through a pulse-shaping filter with impulse response $h_{\text{Tx}}[n]$.

The signal processing node in Fig. 1.4 models the operation of the digital part of the QAM receiver. The simplest receiver performs the following functions:

- recovers the carrier of the transmitter;
- recovers the timing of the transmitter;
- mitigates multipath propagation distortion;
- estimates the correlation of the transmitted signal with a predefined a priori known pattern;
- makes a decision on the value of the transmitted signal; in our case, the distance to the nearest point of the QAM constellation is estimated.

In order to ensure distorting effects compensation possibility, we complete the list of requirements for a complex baseband model of a QAM wireless communication system that must be fulfilled to ensure its relevance:

8. The time variation of the carrier phase difference must be such that it can be considered constant over the impulse responses of the matched filter and equalizer.
9. The rate of dynamic change in the equalizer impulse response must be such that it can be considered constant over the length of the matched filter impulse response.
10. The rate of change of the channel impulse response is less than the rate of the dynamic adjustment of the equalizer impulse response.

Fig. 1.5 shows a system that takes into account the sequence of introducing distortions into the signal and the receiver unit in which these distortions are compensated.

The operation nuances of the described dynamic circuits and the compensated distorting effects are summarized in Table 1.1.

The model described above is used for simulations. In addition, it describes the communication

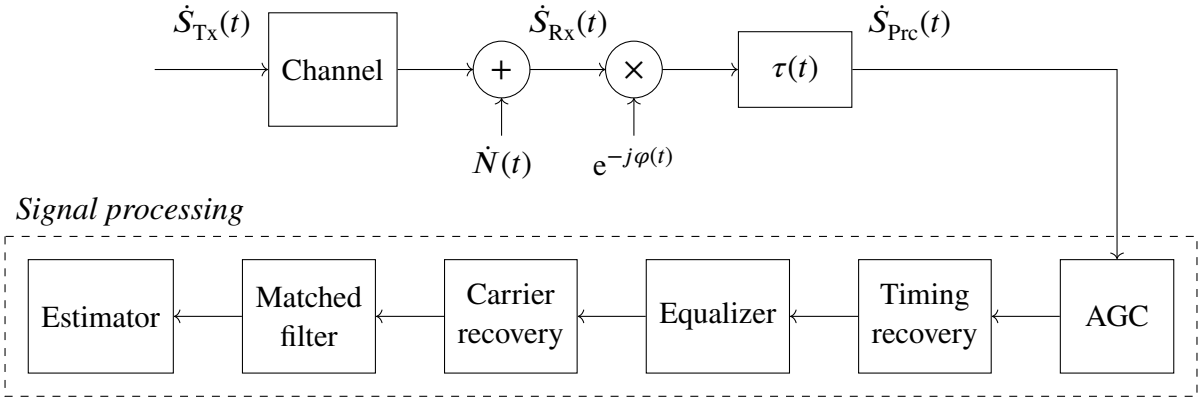

Fig. 1.5. Receiver signal processing block structure

Table 1.1

Summary of the Dynamical Circuits in QAM Receiver

Distorting effect	**Dynamic circuit**	**Compensation**	**Cost function**
Power changes	AGC	$s_{\mathrm{in}}[n]a[n]$, where $a[n]$ is current gain	$\mathbb{E}\left[\lvert\dot{s}_{\mathrm{ex}}[n]\rvert^2\right]$
Modem clock difference	Timing recovery unit	$s_{\mathrm{in}}[n-\tau[n]]$, where $\tau[n]$ is current fractional time shift	$\mathbb{E}\left[s_{\mathrm{ex}} * h_{\mathrm{nb}}[n+1] - s_{\mathrm{ex}} * h_{\mathrm{nb}}[n-1]\right]$, where $h_{\mathrm{nb}}[n]$ is a narrow band filter impulse response
Multipath propagation	Equalizer	$s_{\mathrm{in}}[n] * h[k,n]$, where $h[k,n]$ is current impulse response	Discussed below
Carrier phase difference	Carrier recovery unit	$s_{\mathrm{in}}[n]\,\mathrm{e}^{j\varphi[n]}$, where $\varphi[n]$ is current phase	$\mathbb{E}\left[\arg s_{\mathrm{ex}}[n] - \arg \hat{s}_{\mathrm{ex}}[n]\right]$

system implemented by QAM with high accuracy. For theoretical research, a simplified model was used in the Thesis, which includes:

- symbol generation and zeros insertion;
- combined pulse-shaping of the transmitter filter and the matched filter of the receiver;
- multipath channel passing;
- additive noise;
- equalization;
- carrier recovery and symbol estimation.

The complex baseband model of the QAM wireless communication system shown in Fig. 1.6 is used for theoretical derivations.

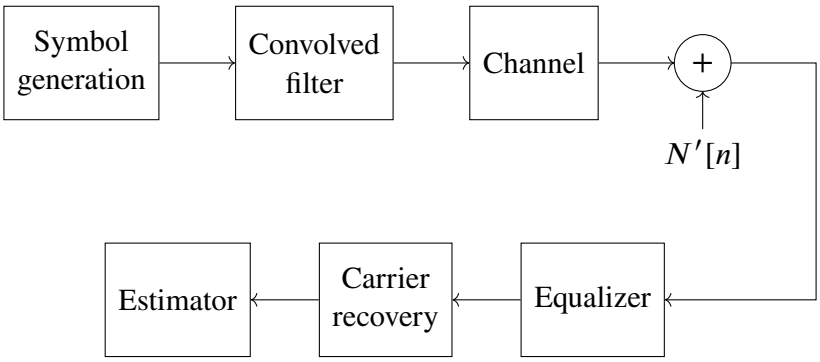

Fig. 1.6. Complex baseband model of QAM communication system for theoretical analysis

1.3 Complex Baseband Multipath Channel Model

To describe the statistical properties of the channel's impulse response, we use a wide-sense stationary uncorrelated scattering (WSSUS) model from [41], [42]. To describe the channel, one should specify multidimensional probability density functions (PDFs) for the system functions. However, the autocorrelation function (ACF) makes it possible to simplify further channel simulation.

The problem of the time-varying channel impulse response generation can be reduced to generating a certain number of random processes to satisfy the covariance matrix $R_{nk}(\Delta t) = R_C[n,k](\Delta t)$ for each time shift Δt. For a simplified solution to this problem, we use the approximation proposed in [43]. It is based on the assumption that the ACF can be separated into two parts in such a way that

$$R_H(\tau, t) = p(\tau)\rho(\Delta t), \tag{1.4}$$

where $p(\tau)$ is the delay-power profile, and $\rho(\Delta t)$ is referred to as spaced-time correlation function. Thus, the covariance matrix can be expressed as a product $\mathbf{R}_C(\Delta t) = \left(R_{nk}\right)\rho(\Delta t)$, where each element is $R_{nk} = R_C[n,k](\Delta t)/\rho(\Delta t)$. The process of generation of channel filter tap $\dot{C}[l](t)$ values is as follows:

- Generate L random processes $\xi_l(t)$ with a complex Gaussian PDF. The one-dimensional ACF of each of the processes corresponds to

$$\rho(\Delta t) = \mathbb{E}\left[\xi_l(t)\xi_l^*(t+\Delta t)\right]. \tag{1.5}$$

  In this case, L is the length of the channel impulse response in samples. The synthesis of non-δ-correlated processes within the framework of this Thesis will be performed using a low-pass filter with an impulse response $h_{\mathrm{D}}[n]$ and a cutoff frequency $f_{\mathrm{c}} = f_{\mathrm{D}}$, where f_{D} stands for the maximum Doppler frequency.
- Introduce cross-correlation into random processes so that the generated L samples correspond to the covariance matrix (R_{nk}) at each time moment t. This problem is solved by multiplying

the vector of samples $\Xi(t)$ by matrix $\mathbf{L}$ for each time moment t.

$$\dot{\mathbf{C}}(t) = \Xi(t)\mathbf{L} = \begin{bmatrix} \xi_1(t) & \xi_2(t) & \cdots & \xi_L(t) \end{bmatrix} \begin{bmatrix} l_{11} & l_{12} & \cdots & l_{1L} \\ 0 & l_{22} & \cdots & l_{2L} \\ \vdots & \vdots & \ddots & \vdots \\ 0 & 0 & \cdots & l_{LL} \end{bmatrix}, \tag{1.6}$$

where $\dot{\mathbf{C}}(t)$ is a $1 \times L$ big vector of band-limited channel impulse response. Matrix $\mathbf{L}$ is calculated by decomposing the covariance matrix using Cholesky factorization $(R_{nk}) = \mathbf{L}\mathbf{L}^{\intercal}$. The decomposition is possible because, due to the properties of the covariance matrix, it is symmetric, real, and positive semi-definite.

The block diagram of the channel is shown in Fig. 1.7. In the figure, $\dot{w}_l[n]$ denotes a discrete complex Gaussian process with zero mean and uniform spectral density.

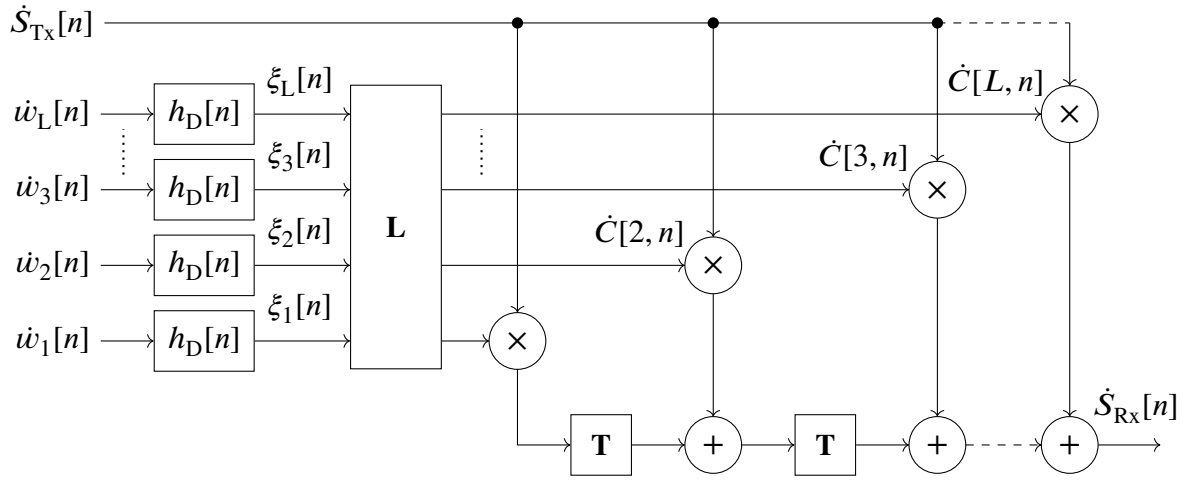

Fig. 1.7. Block diagram of the diffuse multipath chanel

Verification of the algorithms developed in this Thesis will be based on radio-relay data transmission systems. Channel models describing the propagation of radio waves in such data transmission systems assume the presence of a line-of-sight beam.

To describe these phenomena, the Rummler model is used—a multipath model with very slow fading. In terms of the complex envelopes, the model takes the following form:

$$\dot{S}_{\mathrm{Rx}}(t) = \dot{s}_{\mathrm{Tx}}(t) + \alpha \dot{s}_{\mathrm{Tx}}(t-\tau_1)\,\mathrm{e}^{-j2\pi f_0 \tau_1} + \beta \dot{s}_{\mathrm{Tx}}(t-\tau_2)\,\mathrm{e}^{-j2\pi f_0 \tau_2}, \tag{1.7}$$

where f_0 is the carrier frequency.

By limiting the bandwidth of the transmitted signal through Δf, we obtain $\Delta f \tau_1 \ll 1$, which causes flat fading. Therefore, the lowpass-equivalent transfer function can be written as

$$H(f) = 1 + \alpha + \beta\,\mathrm{e}^{-j2\pi f \tau_2}\,. \tag{1.8}$$

In this case, the three-path model is effectively a two-path model.

The lowpass-equivalent channel impulse response, the inverse Fourier transform of the previous frequency response, is

$$h(t) = a[\delta(t) - b\,\mathrm{e}^{-j2\pi(f_0)\tau}\,\delta(t-\tau)]. \tag{1.9}$$

In general, parameters a and b are random and must be measured to ensure model relevance. However, within this Thesis, the channel model will be used to evaluate the ability of an equalizer to converge. Therefore, we consider only the stationary version of this model in further sub-chapters.

1.4 Equalization of QAM Signals

Let us denote the impulse response of the multipath channel through $h[k]$, and the sample of the additive white noise through $n[k]$. Then, one can express the input signal of the equalizer as

$$s_{\mathrm{Rx}}[k] \equiv s_{\mathrm{in}}[k] = \sum_{l_h=0}^{L_h-1} s_{\mathrm{Tx}}[k-l_h]h[l_h] + n[k], \tag{1.10}$$

where L_h is the length of the channel impulse response. The equalizer is a filter with time-varying impulse respone $c[l_c, k]$ of length L_c. By convolving it with input signal (1.10), we can express the equalizer output $s_{\mathrm{ex}}[k]$ as a function of the transmitted signal $s_{\mathrm{Tx}}[k]$:

$$\begin{aligned} s_{ex}[k] &= \sum_{\substack{0\leqslant l_h<L_h \\ 0\leqslant l_c<L_c}} s_{tx}[k-l_h-l_c]h[l_h]c[l_c,k] + n'[k] \\ &= s_{tx}[k-l_\delta] + \sum_{\substack{0\leqslant l<L_h+L_c \\ l\neq l_\delta}} s_{tx}[k-l] \sum_{0\leqslant l_c<l} h[l-l_c]c[l_c,k] + n'[k]. \end{aligned} \tag{1.11}$$

Thus, the output signal of equalizer $s_{\mathrm{ex}}[k]$ is composed of the transmitted signal $s_{\mathrm{Tx}}[k]$ delayed by l_δ and the residual ISI represented by convolution in (1.11).

Consequently, the equalization problem is the adjustment of the tap weights $c[l, k]$ to minimize the effect of the sum in (1.11). To estimate it, the equalizer output dependent cost function $J[k]$ is defined. It is the essence of any blind equalization algorithm.

1.5 Blind Equalization Concept

The CMA is introduced in [2], which states that the variance of the squared output radius $|s_{\mathrm{ex}}[k]|$ has a global minimum at zero ISI. Thus, the cost function for adjusting the equalizer is expressed as follows:

$$J[k] = \mathrm{E}\left[\left(\left|s_{ex}[k]\right|^2 - R^2_{\mathrm{CMA}}\right)^2\right], \tag{1.12}$$

where $\mathrm{E}[\cdot]$ denotes mathematical expectation and R^2_{CMA} is the so-called dispersion constant, which is defined in [2] as

$$R^2_{\mathrm{CMA}} = \frac{\mathrm{E}\left[\left|a_i\right|^4\right]}{\mathrm{E}\left[\left|a_i\right|^2\right]}. \tag{1.13}$$

The equalizer coefficients $c[l,k]$ are adapted using the steepest descent along with $\boldsymbol{J}[k]$, which is approximated by the stochastic gradient $\hat{\nabla}\boldsymbol{J}[k]$. An increment of the equalizer coefficient is expressed by the partial derivative

$$\left.\frac{\partial \boldsymbol{J}[k]}{\partial c}\right|_{c=c[l,k]} = 2\left(\left|s_{\mathrm{ex}}[k]\right|^2 - R^2_{\mathrm{CMA}}\right) s_{\mathrm{ex}}[k] s^*_{in}[k-l], \tag{1.14}$$

where * denotes complex conjugation. Adding it to the current value of $c[l,k]$ gives the next weight of the equalizer tap

$$c[l,k+1] = c[l,k] - \mu\left(\left|s_{\mathrm{ex}}[k]\right|^2 - R^2_{\mathrm{CMA}}\right) s_{\mathrm{ex}}[k] s^*_{in}[k-l], \tag{1.15}$$

where μ is a step-size parameter to regulate the speed of adaptation. Computer simulations in [2] show good convergence properties of CMA.

1.6 Conclusions

In this chapter, the necessary theoretical minimum is provided for discussing blind equalization of QAM signals.

- The band model of a communication system based on QAM is introduced and described.
- The model of the complex baseband of the QAM communication system is described. The criteria necessary for its compliance with the band model are given.
- The sampling criteria for the model of a complex QAM baseband of a communication system are described.
- The blocks for generating the transmitted signal and processing the received signal are considered. The reasons for distorting effects and the possibilities of their compensation are described. The used dynamic loops, the methods of correction application, and the cost functions of these loops are mentioned.
- The models used in this study for simulations and analytical studies are described and constrained.
- The implemented models of multipath channels are described.
- The task of blind equalization is defined, and the equalization process is described. The CMA used for blind equalization of QAM signals is considered, its advantages and disadvantages are emphasized.

2 ENHANCED DECISION-ADJUSTED MODULUS ALGORITHM

2.1 Decision-Adjusted Multimodulus Algorithm

As it comes from (1.15), the goal of the CMA algorithm is positioning all symbols at the output of the equalizer $s_{ex}[k]$ to a single circle, radius R_{CMA} of which is called dispersion constant. The main disadvantage of that approach is the high residual error level. [3] proposes to divide the set of constellation points $\{a_m\}$ into subsets with the same radius R_i:

$$\{a_m\} = \bigcup_i \left\{ a_m \middle| |a_m| = R_i \ \forall\ m \right\}_i . \tag{2.1}$$

As a result, the proposed algorithm, DAMA, implements a CMA for each constellation circle. Equalizer coefficients updates are expressed as:

$$c[l, k+1] = c[l, k] - \mu \left(\left| s_{ex}[k] \right|^2 - R_i^2 \right) s_{ex}[k] s_{in}^*[k-l], \tag{2.2}$$

where the dispersion constant for each output radius $s_{ex}[k]$ value is such that its deviation from R_i is minimal $\min\limits_i \left| \left| s_{ex}[k] \right|^2 - R_i^2 \right|$.

Unlike CMA, when the equalizer is converged, the increments of its coefficients are equal to zero $\forall s_{tx}[k] \in \{a_n\}\ \exists!\ R_i : \left| s_{tx}[k] \right|^2 = R_i^2$. Thus, DAMA is proposed to provide residual error significantly lower than CMA.

2.2 Error Statistical Properties

The testing setup to provide data for numerical verification is shown in Fig. 2.1.

The setup consists of:

- data generator, mapper, and low pass filter;
- testing channel; fractional delay filter and narrow band-pass filter (BPF) for fractional delay synchronization; and maximum selector and correlator integer delay synchronization;
- PDF estimator and Pearson criterion estimator.

The Pearson's chi-squared test is used to determine whether the error distribution for real data is sufficiently close to normal or not. The number of histogram bins for simulation is chosen equal to $K_1 = 100$, whereas the number of processed symbols, i.e., sample size is $K_2 = 100\,000$. After the simulation is finished, the Pearson criterion estimation block computes χ^2_{ev}-level to compare it to the critical value. Therefore, the only evaluated parameter is standard deviation, and for the given number of histogram bins $K_1 = 100$ the number of degrees of freedom is $K_3 = K_1 - 2 = 98$. Assuming the confidence level $\gamma = 0.95$, to accept the hypothesis that distribution is normal, evaluated

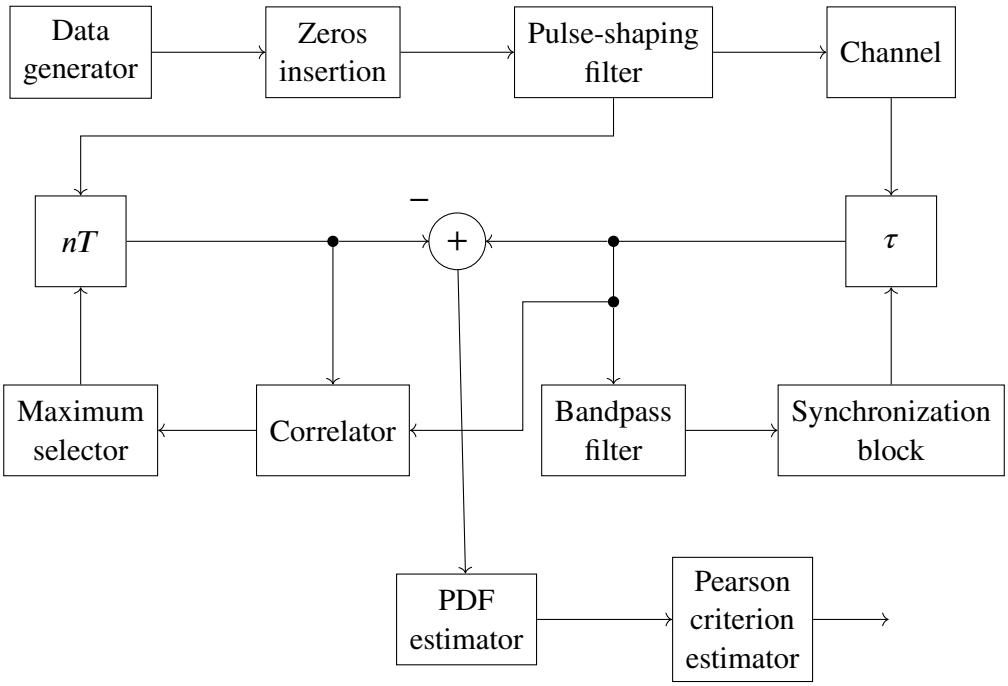

Fig. 2.1. Distribution analysis setup

parameter χ^2_{ev} should be less than the critical level $\chi^2_{\text{cr}} = 122.1077$. If the error's both real and imaginary parts met the criterion, the system forms *passed* the test marker.

Simulation was performed repeatedly $K_4 = 100$ times for different depth and frequency notches.The simulation results are summarized in Table 2.1.

Table 2.1

Distribution Verification Results

	Passed test percentage					
f_nT	1 dB	5 dB	10 dB	15 dB	20 dB	25 dB
-0.25	97	95	98	97	100	96
-0.20	97	96	96	100	97	99
-0.15	98	96	97	96	96	96
-0.10	99	97	100	96	99	99
-0.05	97	97	98	98	99	100
0.00	99	96	99	98	96	99
0.05	99	99	98	99	96	95
0.10	97	97	96	96	95	97
0.15	97	99	96	98	98	99
0.20	98	99	96	100	96	98
0.25	96	100	100	96	99	98

2.3 Enhanced DAMA

The PDF of radial error has shifted Ricean distribution $\varphi_n(R_n, \sigma) = \varphi(R_n, \sigma) - R_n$, where $\varphi(R_n, \sigma)$ is Ricean distribution with deviation σ and R_n is the n-th radius in the constellation. We also denote m_n a number of constellation points of radius equal to R_n.

Assume all constellation points can be divided to N groups of constant radii R_n, $n = 1 \dots N$. The number of points in each of these groups is given by m_n. Apparently, the possibility that arbitrary point belongs into n-th group is expressed by

$$P_n = \frac{m_n}{M}, \tag{2.3}$$

where M is overall number of constellation points.

Assume, as it was previously, that it is the sample of radius R_x and two nearest radii R_{n-1} and R_{n-1} satisfy inequality $R_{n-1} \leq R_x < R_n$. Obviously, the possibility that the sample of radius R_x is caused be the symbol of radius other than R_{n-1} or R_n is smaller of these two. If it was the symbol of radius $R > R_n$, detection of R_n ensures correct equalizer adjustment. And otherwise, if the symbol in the detector is assumed of radius R_{n-1}, it will cause misadjustment. Among a number of all possible error types we will observe only

$$\{P_{n-1,k} | k = n \dots N\} \quad \text{and} \quad \{P_{n,k} | k = 1 \dots n-1\}. \tag{2.4}$$

Obviously, the first group of errors in the previous equation causes positive adjustment error and the second one—negative error. Therefore, possibilities of these errors can be expressed as

$$P_{n-1,k} = \int_{-\infty}^{R_{\text{th}\,n-1}} \varphi(R_n, \sigma) \mathrm{d}R, \quad k = n \dots N \tag{2.5}$$

for positive and

$$P_{n,k} = \int_{R_{\text{th}\,n-1}}^{\infty} \varphi(R_{n-1}, \sigma) \mathrm{d}R, \quad k = 1 \dots n-1 \tag{2.6}$$

for negative ones. Assuming risk coefficients for all error types equal to $r_{n-1,k} = r_{n,k} = 1$ yields to the following overall risk expression

$$r = \sum_{k=1}^{n-1} P_{n,k} P_k + \sum_{k=n}^{N} P_{n-1,k} P_k. \tag{2.7}$$

Acting like previously, let us express $P_{n-1,k} = 1 - P_{k,k}$, where $k = n \dots N$. Note also that $P_{k,k}$ can be calculated integrating $\varphi(R_k, \sigma)$ from $R_{\text{th}\,n-1}$ to the infinity. Thus, overall risk expression can be

rewritten:

$$r = \sum_{k=n}^{N} P_k - \int_{R_{\text{th}\,n-1}}^{\infty} \left[\sum_{k=n}^{N} \varphi(R_k, \sigma) P_k - \sum_{k=1}^{n-1} \varphi(R_k, \sigma) P_k \right] \mathrm{d}R. \tag{2.8}$$

Integral value maximization is performed in the same manner as in the case of two radii, i.e., defining the integration interval so that the integrand is positive. Therefore, the threshold level is obtainable by the computation R location where inequality

$$\sum_{k=n}^{N} \varphi(R_k, \sigma) P_k \geq \sum_{k=1}^{n-1} \varphi(R_k, \sigma) P_k \tag{2.9}$$

becomes true. Calculating threshold level in this manner we decrease the wrong detection possibility and therefore the equalizer misadjustment possibility. In Fig. 2.2, the 32-QAM constellation is shown as well as calculated thresholds.

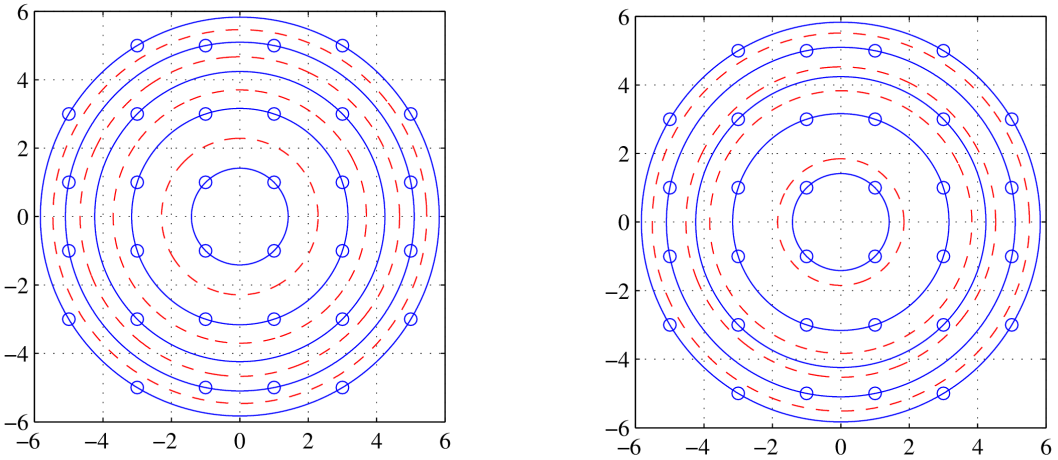

(a) DAMA (b) EDAMA multilevel

Fig. 2.2. Constellations and thresholds for (a) CMA, (b) DAMA, (c) EDAMA 2-level, and (d) EDAMA multilevel equalization algorithms

2.4 Simulation Results

The performance of the proposed algorithm was tested through simulations in the Matlab environment. The signal shaping at the equalizer input corresponds to the communication system model described in Section 1.2. The user signal is generated based on 32-QAM modulation. The equalizer is a 33-tap half-baud finite impulse response filter with dynamically adjustable gains. In the experiments, CMA, DAMA, and enhanced decision-adjusted modulus algorithm (EDAMA) objective functions were used to adjust the weights of the equalizer taps.

Obtaining convergence curves allows one to clearly demonstrate the convergence rate of the proposed algorithm and the level of residual error. It was noted above that in the case of EDAMA, the

level of residual error is significantly lower compared to CMA. On the other hand, EDAMA should show faster convergence than DAMA. 10 dB and 15 dB notch channels were applied to emulate multipath propagation. Simulation results for the case of 10 dB notch channel are shown in Fig. 2.3.

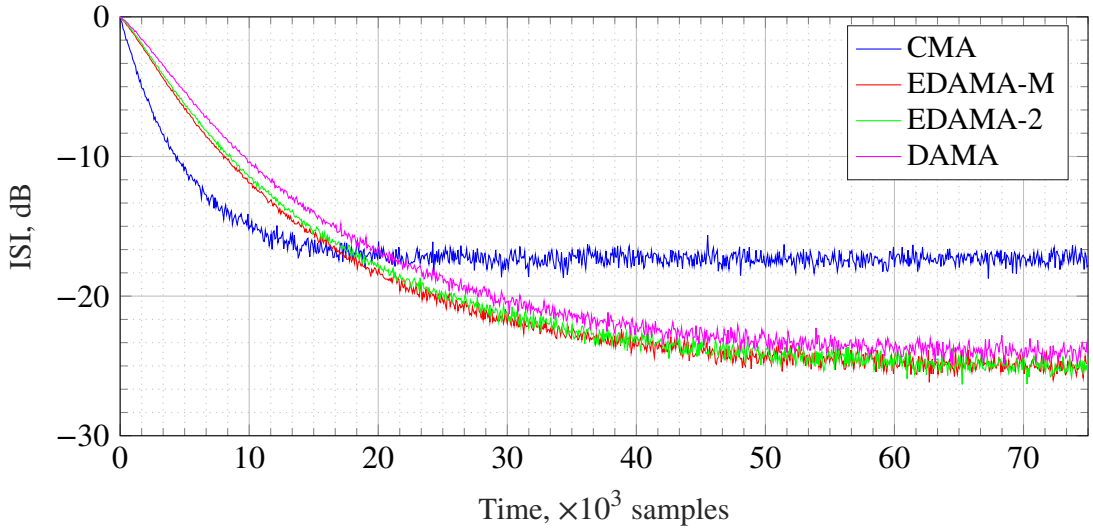

Fig. 2.3. Convergence curve for EDAMA in the case of 10 dB notch channel

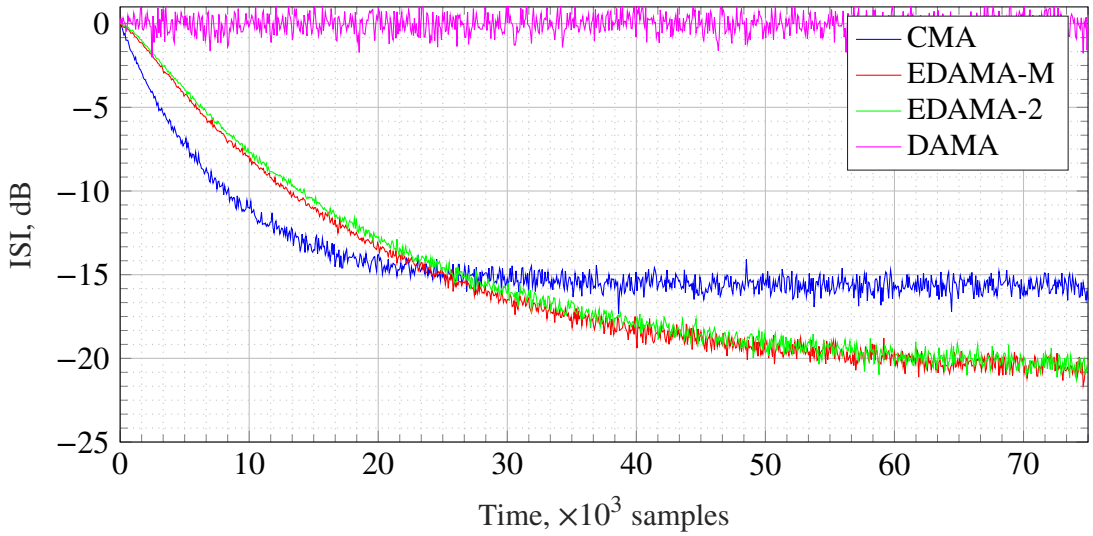

Fig. 2.4. Convergence curve for EDAMA in the case of 15 dB notch channel

According to the simulation results, CMA is the fastest equalization algorithm, showing the highest residual error level. EDAMA for the implemented channels showed the lowest steady-state intersymbol interference level. As postulated, this algorithm ensures faster convergence compared to DAMA. Worth noting that EDAMA with thresholds computed by the multiple radii approach (EDAMA-M) appeared faster than when the two radii approach performed computation. In the case of 15 dB deep notch channel, the DAMA algorithm was not able to converge. Concluding, EDAMA showed better performance than the classically used CMA method without losing the ability of deep

notch acquisition.

2.5 Conclusions

The goal of this chapter was to propose a blind equalization algorithm for QAM signals that provides a reduced level of residual error at the output of the equalizer. The following milestones were passed in the course of this task.

- The DAMA for blind equalization of QAM signals was described. The cost function of the algorithm was considered in terms of the decision threshold values.
- The PDF of the deviation of the signal point at the output of the equalizer from the value of the radius of the transmitted symbol was considered. The correspondence between the PDF of this variable and the shifted Rice distribution was shown.
- Two-radius and multi-radius approaches were proposed for calculating the optimal thresholds for deciding on the received symbol. Optimal thresholds improve the cost function for adjusting the equalizer in EDAMA.
- An increase in the equalizer's ability to converge was demonstrated, associated with a decrease in the error probability in decision making.
- A decrease in residual error level was demonstrated, compared to CMA, in the case of limited equalizer length and a non-zero noise level.
- Zero residual error was shown for an infinite equalizer filter length and if its impulse response matched the channel.

3 GROUPED RADII APPROACH

3.1 An Impact of Detection Error Probability on the Convergence of Equalizer

Updates to the weights of the equalizer taps for EDAMA are expressed as

$$c[l,k+1]=c[l,k]- \\ -\mu\left(\left|s_{ex}[k]\right|^2-R^2\right)\Big|_{R:\ |\hat{s}_{tx}[k]|=R} s_{ex}[k]s_{in}^*[k-l]. \tag{3.1}$$

Consider the case of the symbol misestimation. It happens when the output radius has deviated beyond the detection threshold $|s_{ex}[k]| > T_i$. If $|s_{ex}[k]|$ has not reached the radius of the next circle R_{i+1}, the expression $\left(\left|s_{ex}[k]\right|^2 - R^2\right)\Big|_{R=R_{i+1}}$ becomes of the opposite sign. Therefore, all equalizer taps move in the direction opposite to the true one. If the deviation has exceeded the distance between the radii, erroneous detection does not necessarily cause weights misadjustment. The lower deviation is more likely to happen, so the number of misadjustments in the case of erroneous symbol estimation is greater. Convergence remains possible as long as the number of misadjustments allows to omit averaging in the steepest descent of the cost function (1.12) and approximate it with a stochastic gradient $\hat{\nabla} J[k]$.

3.2 Detection Error Probability as a Function of Output Radius Variance

In this section, the effect of the output radius variance on the misadjustment probability is analyzed. In [38], it is shown that the deviation $s_{ex}[k]-s_{tx}[k-l_\delta]$ caused by ISI has a normal distribution for the channels used. Therefore, the output radius $R = |s_{ex}[k]|$ has a Ricean distribution $\varphi\left(R|R_i,\sigma_R\right)$, where R_i is the original symbol radius, and σ_R is the standard deviation.

Let us assume that $M_i = \left|\{a_m\}_i\right|$ is the number of points on the ith circle, and M is the total number of constellation points. Then, their ratio is equal to the probability of transmitting a symbol from this circle $P(R_i) = M_i/M$. The probability that the radius R_i at the output of the equalizer becomes R is equal to

$$P(R|R_i) = \lim_{\Delta R\to 0} \int_{R-\Delta R/2}^{R+\Delta R/2} \varphi\left(R|R_i,\sigma_R\right) \mathrm{d}R. \tag{3.2}$$

Assume that the output radius R belongs to the detection area of the ith constellation circle $R \in [T_i, T_{i+1})$. An estimation will be correct if a point from $\{a_m\}_i$ has been transmitted. If a point from any other constellation circle has caused the output radius R, an estimation block will make an error. Thus, according to the law of total probability, the probability of misestimation $P_{\text{er}}(R)$ can be expressed as

$$P_{\text{er}}(R) = \sum_{k\neq i} P(R_k)P(R|R_k). \tag{3.3}$$

The substitution of (3.2) in (3.3) and changing summation and integration order allows expressing error probability

$$P_{\text{er}}(R) = \lim_{\Delta R \to 0} \int_{R-\Delta R/2}^{R+\Delta R/2} \sum_{k \neq i} P(R_k) \varphi\left(R | R_k, \sigma_R\right) \mathrm{d}R. \tag{3.4}$$

Let us call the integrand the probability density function (PDF) of the estimation error

$$\varphi_{\text{er}}(R|\sigma_R) = \sum_{k \neq i} P(R_k) \varphi\left(R | R_k, \sigma_R\right). \tag{3.5}$$

In Section 3.1, it was mentioned that an estimation error does not necessarily lead to the weights misadjustment. Let us now express the probability of such an event:

$$\varphi_{\text{mis}}(R|\sigma_R) = \begin{cases} \sum\limits_{k<i} P(R_k) \varphi\left(R | R_k, \sigma_R\right) & \text{if } R \in [T_i, R_i) \\ \sum\limits_{k>i} P(R_k) \varphi\left(R | R_k, \sigma_R\right) & \text{if } R \in [R_i, T_{i+1}). \end{cases} \tag{3.6}$$

Fig. 3.1 shows the dependence of $\varphi_{\text{mis}}(R|\sigma_R)$ on the deviation R for different values of standard deviation σ_R. Detection areas are marked with alternating gray and white stripes. The blue lines represent the radii R_i of the circles. Like the PDF of misestimation $\varphi_{\text{er}}(R|\sigma_R)$, the PDF of misadjustment $\varphi_{\text{mis}}(R|\sigma_R)$ rapidly grows up near the closely positioned circles of the constellation.

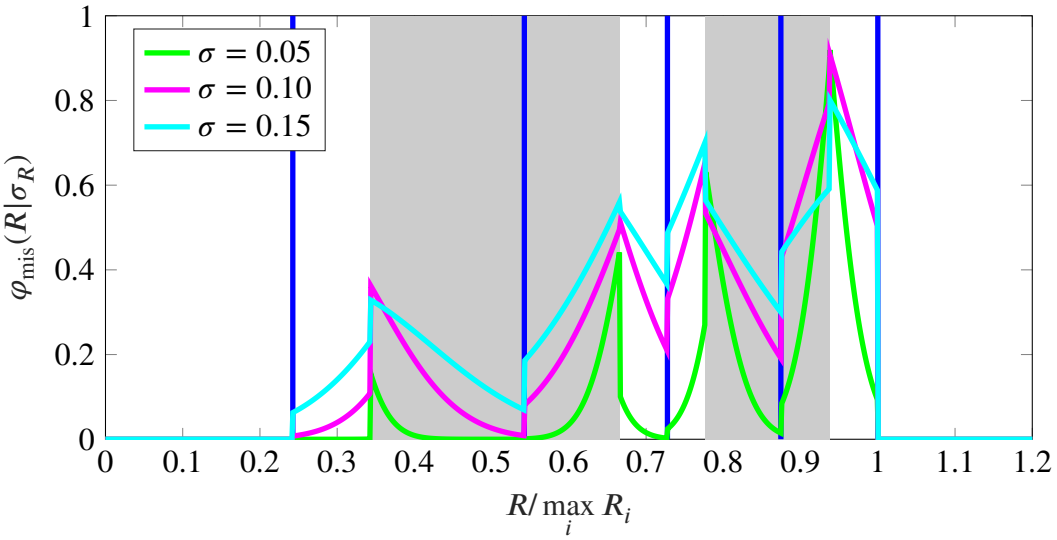

Fig. 3.1. The equalizer misadjustment PDF $\varphi_{\text{mis}}(R|\sigma_R)$

3.3 Proposed Optimization Procedure

The proposed approach aims to reduce the probability of the dispersion (1.12) growth in case of misestimation. The procedure also allows customizing the algorithm to ensure optimal performance

for a fixed σ_R.

Assume the circles $\{a_m\}_i$ and $\{a_m\}_{i+1}$ of the constellation $\{a_m\}$ are the most closely positioned to each other, i.e., the radii R_i and R_{i+1} of these circles are such that $\min\limits_k \left(R_{k+1} - R_k\right) = R_{i+1} - R_i$. The idea of the proposed procedure is to combine the points of these two circles into a single subset $\{a_m\}_j = \{a_m\}_i \cup \{a_m\}_{i+1} \subset \{a_m\}$ (note the change in the subset indexing).

Like in the DAMA and EDAMA algorithms, each subset of the constellation points has its detection area. If the output radius R falls within the $\{a_m\}_j$ detection zone, the adaptation mechanism works like CMA, i.e., tries to minimize dispersion for points in this zone. Recall, (1.15) says that the CMA tries to pull the squares of the radii $|s_{ex}[k]|^2$ of all constellation points to one single value R^2_{CMA}. It ensures a minimum of dispersion. Similarly, the proposed algorithm tries to pull the squares of the radii of points $\{a_m\}_j$ to the corresponding R_j^2. According to the method we have used to calculate (1.13), one can express the dispersion constant for subset $\{a_m\}_j$:

$$R_j^2 = \frac{\mathrm{E}\left[|a|^4\right]}{\mathrm{E}\left[|a|^2\right]} \quad \forall a \in \{a_m\}_j. \tag{3.7}$$

The dispersion constants R_j^2 must be calculated for all subsets $\{a_m\}_j$ formed by the union of the circles $\{a_m\}_i$:

$$\{a_m\}_j = \bigcup_{k=i}^{i+K-1} \{a_m\}_k, \tag{3.8}$$

where $K \geqslant 1$ is the number of united circles. For the subsets coinciding with the circles $\{a_m\}_j = \{a_m\}_i$, the dispersion constant R_j^2 is equal to the squared radius R_i^2 of the points on this circle. The subsets can also be formed by combining points of more than two adjacent circles ($K > 2$).

Consider the range of the output radii to which the detection threshold belongs $T_i \in [R_i, R_{i+1})$. Assume one has transmitted a point from the subsets $\bigcup\limits_{k>i} \{a_m\}_k$ or $\bigcup\limits_{k\leqslant i} \{a_m\}_k$. If the output radius falls below the threshold $R \in [R_i, T_i)$ or rises above the threshold $R \in [T_i, R_{i+1})$, respectively, a misadjustment will occur. Taking into account the probability of transmission a point from the ith constellation circle $P(R_i) = |\{a_m\}_i|/|\{a_m\}|$, the misadjustment probability is

$$P_{\text{mis}} = \sum_{k>i} P(R_i|R_k)P(R_k) + \sum_{k\leqslant i} P(R_{i+1}|R_k)P(R_k), \tag{3.9}$$

where $P(R_i|R_k)$ and $P(R_{i+1}|R_k)$ are the probabilities that the output radius R caused by a point from the kth circle will belong to the ranges $R \in [R_i, T_i)$ and $R \in [T_i, R_{i+1})$, respectively, i.e., will be interpreted as a symbol from the ith or the $(i+1)$th circle.

Since the PDF of the output radius caused by a point from the kth circle is $\varphi\left(R|R_k, \sigma_R\right)$, prob-

ability $P(R_i|R_k)$ can be calculated as follows:

$$\begin{aligned} P(R_i|R_k) &= \int_{R_i}^{T_i} \varphi\left(R|R_k,\sigma_R\right)\,\mathrm{d}R \\ &= Q_1\left(\frac{R_k}{\sigma_R},\frac{R_i}{\sigma_R}\right) - Q_1\left(\frac{R_k}{\sigma_R},\frac{T_i}{\sigma_R}\right), \end{aligned} \tag{3.10}$$

where Q_1 is the Marcum Q-function. The second group of probabilities $P(R_{i+1}|R_k)$ is calculated similarly:

$$P(R_{i+1}|R_k) = Q_1\left(\frac{R_k}{\sigma_R},\frac{T_i}{\sigma_R}\right) - Q_1\left(\frac{R_k}{\sigma_R},\frac{R_{i+1}}{\sigma_R}\right). \tag{3.11}$$

The substitution of (3.10) and (3.11) into (3.9) gives

$$\begin{aligned} P_{\text{mis}}(T_i) &= \sum_{k\leqslant i} Q_1\left(\frac{R_k}{\sigma_R},\frac{T_i}{\sigma_R}\right)P(R_k) \\ &- \sum_{k>i} Q_1\left(\frac{R_k}{\sigma_R},\frac{T_i}{\sigma_R}\right)P(R_k) + P'_{\text{const}}, \end{aligned} \tag{3.12}$$

where P'_{const} is independent from T_i. An optimization criterion for the detection thresholds T_i is a minimum of the misadjustment probability. Thus, the problem is reduced to finding the extremum $\min\left[P_{\text{mis}}(T_i)\right]$, varying T_i in the range of $[R_i, R_{i+1})$.

Consider an example of the described approach. Fig. 3.2 exposes the misadjustment PDF $\varphi_{\text{mis}}\left(R|\sigma_R\right)$ for different standard deviation σ_R values. As in the case shown in Fig. 3.1, the algorithm used 32-QAM modulation. Notice a union of points of the 3rd, 4th, and 5th circles into one subset. Detection areas are marked with alternating gray and white stripes. The solid blue lines represent the dispersion constants R_j, and the dashed lines denote the radii, R_i, of the circles.

Comparing the misadjustment PDFs $\varphi_{\text{mis}}(R|\sigma_R)$ near the closely positioned constellation circles, it becomes apparent that the proposed algorithm significantly reduces the risk of dispersion growth at the equalizer output.

3.4 Simulation results

Simulations verified the performance and convergence properties of the proposed algorithm. The signal forming at the equalizer input corresponds to the communication system model described in Section 1.2. The transmitting signal was generated using standard 32-QAM and 64-QAM constellations. According to the previously described communication system model, the signal forming block incorporated the transmitter's pulse-shaping and the receiver's matched filters. The multipath phenomenon emulation was performed using a two-ray propagation model described in Section 1.3. The depth of the notch utilized as the channel was equal to 10 dB and 15 dB. White Gaussian noise

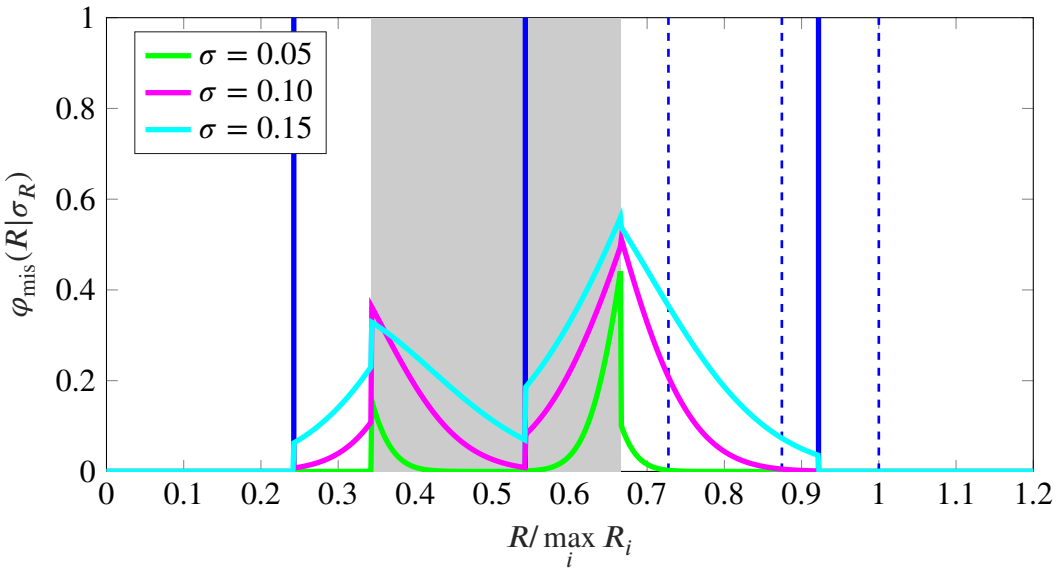

Fig. 3.2. The misadjustment PDF $\varphi_{\text{mis}}(R|\sigma_R)$ for the united 3rd, 4th, and 5th circles of the 32-QAM constellation

has been added to the signal to provide a signal-to-noise ratio of 35 dB at the equalizer input.

Convergence curves show the dependence of residual error on the iteration number. The error is expressed as the difference between the equalizer output signal radius and the radius of the estimated symbol $\big||s_{ex}[k]|-|\hat{s}_{tx}[k]|\big|$. For each set of system parameters and each algorithm, 200 Monte Carlo simulations were performed. The resulting curves were obtained by averaging them.

Fig. 3.3 shows the simulation result for a 32-QAM signal with the 10 dB deep notch channel for multipath propagation emulation. It shows convergence curves for CMA, EDAMA, and the constellation points grouping algorithm. The presented algorithm combines $i \in \{3;4;5\}$ circles of the 32-QAM constellation. In the figure, it is designated as TEST.

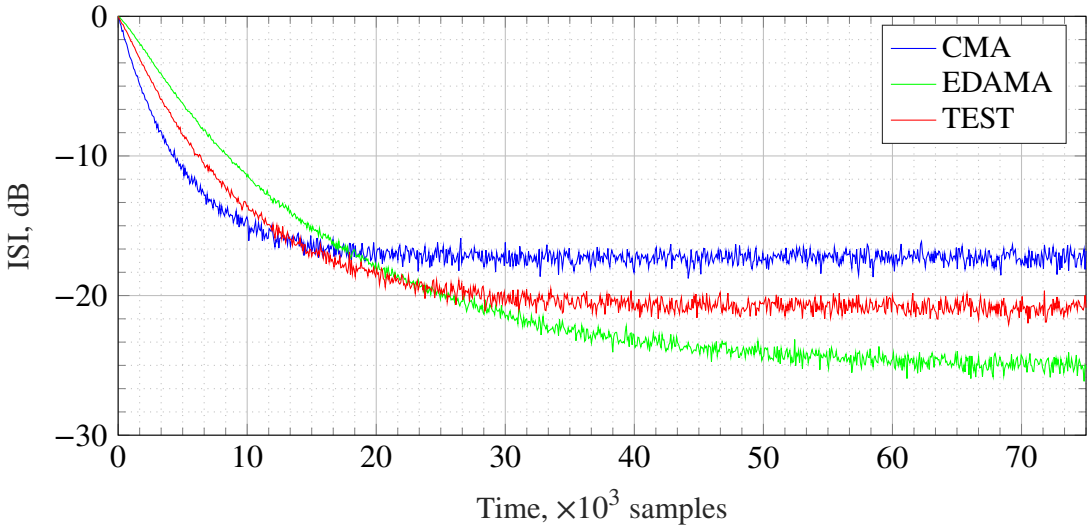

Fig. 3.3. Convergence curves for CMA, EDAMA, and the proposed algorithm in the case of the 10 dB notch channel

The convergence curves confirm that the constellation points grouping algorithm converges faster than EDAMA because of fewer detection errors at the initial adaptation stage. On the other hand, its intersymbol interference is lower than CMA due to the split dispersion constants.

Further, Fig. 3.4 shows the convergence curves for 64-QAM modulation and 15 dB deep notch. It also compares CMA, EDAMA and the proposed algorithm. The last one unifies $i \in \{3; 4; 5\}$ circles and $i \in \{6; 7; 8\}$ circles of the constellation. In the figure, it is designated as TEST.

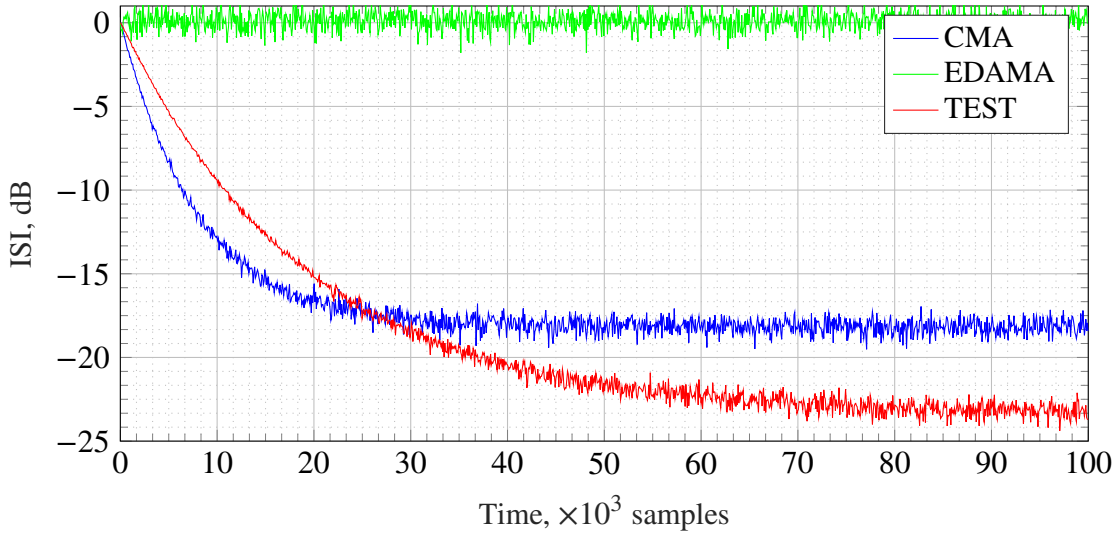

Fig. 3.4. Convergence curves for CMA, EDAMA and the proposed algorithm in the case of 15 dB noth channel

The proposed algorithm converged more slowly than the CMA but ensured much lower residual ISI. Due to the high number of misadjustments, EDAMA did not converge at all.

3.5 Conclusions

This chapter was devoted to cracking the equalizer convergence complexity problem due to the high level of variance of the signal at the output of the equalizer. A solution has been proposed using conditional probability distributions and grouping constellation circles. The following points should be noted summarizing the results obtained.

- A relationship has been shown between the probability of erroneous detection and the ability of an equalizer to converge.
- The concept of conditional probability density was introduced, and its application to optimization of the cost function was shown.
- It has been demonstrated that the probability of misestimation and the probability of misadjusting equalizer weights are not equivalent. The adjustment may be correct in case of an incorrectly detected symbol.
- An increased probability of equalizer misadjustment in intervals with closely spaced constellation circles has been demonstrated.

- An approach to group points from nearby circles of the constellation has been proposed. It allowed adjusting the cost function to reduce the variance of the equalizer output signal if the signal point belonged to the interval between these circles.
- Simulations using the proposed approach have shown that the equalizer gains the ability to converge under conditions in which it is not possible in the case of EDAMA.

4 ADAPTIVE SWITCHED GR-DAMA APPROACH

4.1 Error Measurement Methods

It was mentioned that the received signal is a weighted sum of the delayed replicas of a transmitted signal. Indeed, (1.11) shows that the output signal of the equalizer $s_{ex}[k]$ is a convolution of the transmitted signals $s_{tx}[k]$ with the convoluted impulse responses of channel $h[k]$ and equalizer $c[l,k]$. Thus, from the essence of the convolution process, each output sample can be expressed as a linear combination of the neighboring symbols in the transmitted signal $\{\dots, s_{tx}[k-1], s_{tx}[k], s_{tx}[k+1], \dots\}$

$$s_{ex}[k] = \sum_{l=0}^{L_c+L_h-1} (h * c[k])[l] s_{tx}[k-l], \tag{4.1}$$

where L_c and L_h are lengths of the channel and equalizer impulse responses, respectively.

As changes in the channel and adaptation of the equalizer are relatively slow, signal $s_{ex}[k]$ can be assumed locally ergodic. Thus, the variance of the signal can be calculated, taking into account that the symbols are uncorrelated:

$$E\left[|s_{ex}[k]|^2\right] = E\left[|s_{tx}[k]|^2\right] \sum_{l=0}^{L_c+L_h-1} |(h * c[k])[l]|^2. \tag{4.2}$$

For the ideal compensation, $E\left[|s_{ex}[k]|^2\right] = E\left[|s_{tx}[k]|^2\right]$. If the ISI is presented in the signal, the central coefficient of the $(h * c[k])[l]$ is still unweighted $\delta[k]$. Thus, the output radius variance $E\left[|s_{ex}[k]|^2\right]$ is minimal for the mitigated ISI. The variance of noise $E\left[|n'[k]|^2\right]$, as it is not correlated with the transmitted symbols, is appended to the variance of the data signal. Thus, variance indicates the amount of the ISI and noise in the signal. To construct probability densities of the received signal, one has to assess its parameters. In the case of the Ricean distribution, mean values correspond to the radii of the constellation circles. The standard deviation can be estimated from the received signal variance

$$\hat{\sigma}_R = \sqrt{E\left[|s_{ex}[k]|^2\right] - E\left[|s_{tx}[k]|^2\right]}, \tag{4.3}$$

where $E\left[|s_{ex}[k]|^2\right]$ can be calculated from the equalizer output signal and $E\left[|s_{tx}[k]|^2\right]$ is a predefined constant.

Section 3.2 described the dependence of the misadjustment probability density on the standard deviation of the noisy process in the signal. The calculation of the misadjustment probability

$P_{\text{mis}}(\sigma_R)$ is possible through the integration of (3.6):

$$
\begin{aligned}
P_{\text{mis}}(\sigma_R) &= \int_0^{\infty} \varphi_{\text{mis}}(R|\sigma_R)\,\mathrm{d}R = \\
&= \sum_j \sum_{k:\,R_k<R_j} P(R_k)\left[Q_1\left(\frac{R_k}{\sigma_R},\frac{R_j}{\sigma_R}\right) - Q_1\left(\frac{R_k}{\sigma_R},\frac{T_j}{\sigma_R}\right)\right] + \\
&+ \sum_j \sum_{k:\,R_k>R_j} P(R_k)\left[Q_1\left(\frac{R_k}{\sigma_R},\frac{T_{j+1}}{\sigma_R}\right) - Q_1\left(\frac{R_k}{\sigma_R},\frac{R_j}{\sigma_R}\right)\right],
\end{aligned}
\tag{4.4}
$$

where Q_1 is the Marcum Q-function; summation by j is performed among all subsets $\{a_m\}_j$, and summation by k—among all constellation circles $\{a_m\}_i$.

Fig. 4.1 shows the misadjustment probability $P_{\text{mis}}(\sigma_R)$ dependence on the standard deviation in the Ricean probability density σ_R. Blue, red, green, and magenta lines denote curves for the generalized EDAMA of two, three, and four subsets of points and standard EDAMA algorithms, respectively. Dotted black lines indicate standard deviation σ_R values in which $P_{\text{mis}}(\sigma_R) = 2\,\%$. For high variance values, only CMA algorithm is capable of equalizer adaptation with zero misadjustment probability. After equalizer sets have been partially adjusted, the output radius variance decreases, and two subset generalized EDAMA algorithm can now operate with $P_{\text{mis}}(\sigma_R) \leqslant 2\%$. Further adjustment of the tap weights leads to the ability of the two subset generalized EDAMA algorithm to converge equalizer. Thus, the adaptation process evolves from the CMA algorithm to the EDAMA algorithm. As throughout the adaptation $P_{\text{mis}}(\sigma_R)$ is kept low, the proposed approach demonstrates convergence abilities comparable to ones of the CMA; on the other hand, in the steady state, residual error is the same as for the EDAMA algorithm.

4.2 Simulation Results

Simulations verified the performance and convergence properties of the proposed algorithm. The signal forming at the equalizer input corresponds to the communication system model described in Section 1.2. The transmitting signal was generated using standard 32-QAM constellations. According to the previously described communication system model, the signal forming block incorporated the transmitter's pulse-shaping and the receiver's matched filters. The multipath phenomenon emulation was performed using a two-ray propagation model described in Section 1.3. The depth of the notch utilized as the channel was equal to 10 dB and 15 dB.

The results of the simulations are illustrated with convergence curves, which show the dependence of the residual error on the iteration, or clock cycle, number. The residual error, in this case, is calculated as the difference between the output radius and the radius of the estimated symbol. For each parameter set, 200 Monte Carlo runs of the simulations were performed.

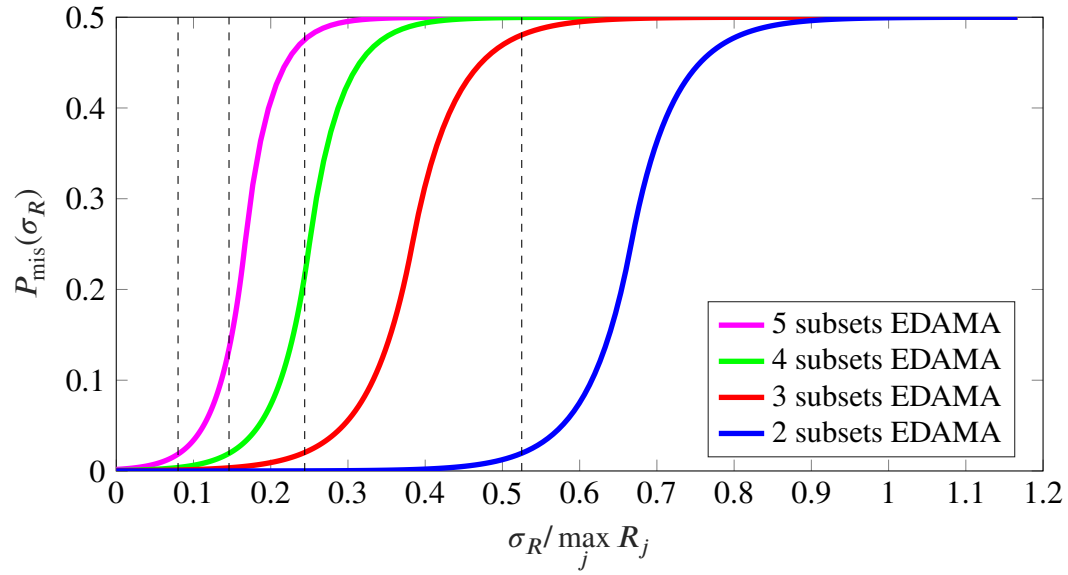

Fig. 4.1. Misadjustment probability $P_{\text{mis}}(\sigma_R)$ dependence on the standard deviation σ_R of noise-like signal

Fig. 4.2 shows the simulation results for the 10 dB deep notch blind equalization in the case of 32-QAM signal. The switching threshold is chosen to ensure the misadjustment probability $P_{\text{mis}}(\sigma_R) = 2\,\%$.

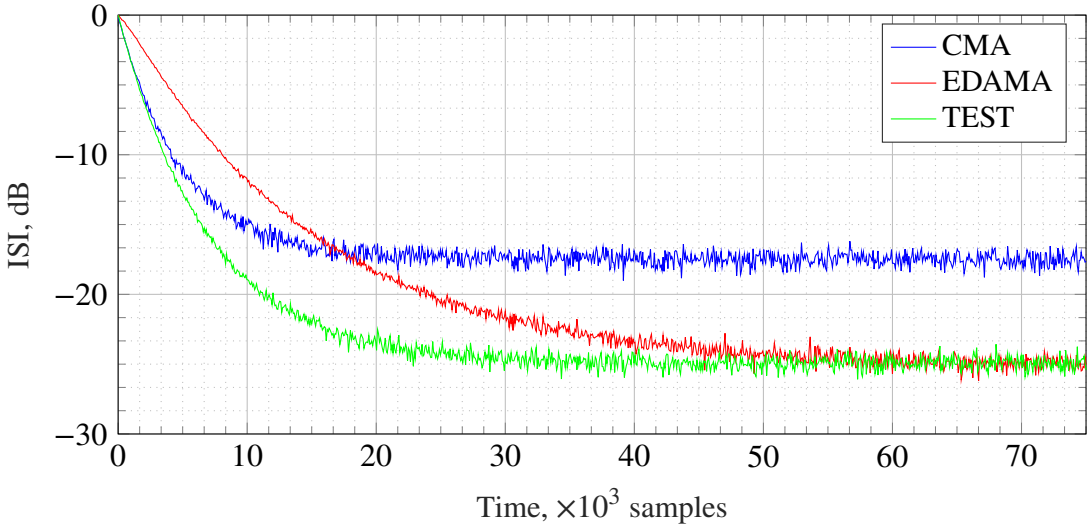

Fig. 4.2. Equalizer convergence plots for CMA, EDAMA, and the switching approach for the 10 dB deep notch channel

The experiments show that the switching approach ensures low residual error, as at the final stage of this algorithm it uses the EDAMA cost function. On the other hand, it converges much faster because of the lower number of misadjustments at the initial stages.

In the second experiment, the same signal has been passed through the channel represented by a 20 dB deep notch. The convergence curves for this simulation are given in Fig. 4.3. As previously, the misadjustment probability is kept $P_{\text{mis}}(\sigma_R) = 2\,\%$.

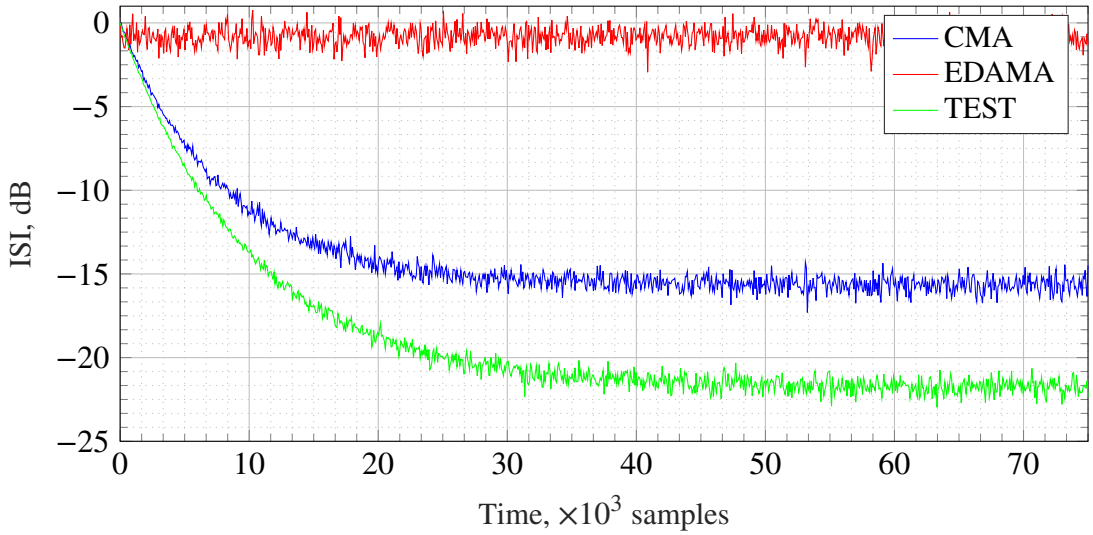

Fig. 4.3. Equalizer convergence plots for CMA, EDAMA, and the switching approach for the 15 dB deep notch channel

As previously, the switching approach converged with lower residual ISI comparing to the CMA. Notably, the EDAMA algorithm failed to converge because of high misadjustment probability. On the other hand, as the proposed approach's final stage, EDAMA ensured low residual error.

4.3 Conclusions

This chapter is devoted to the possibility of using blind equalization algorithms that are best suited to the current channel parameters and the degree of equalizer adjustment. In summary, the following considerations should be noted.

- It has been shown that for each unique union of adjacent constellation circles, the dependence of the probability of misadjustment of the equalizer is a monotonic growing function of the standard deviation.
- It has been demonstrated that the set of unique unions of adjacent constellation circles can be ordered so that the probability of misadjustment of the equalizer for each successive algorithm is greater for the same value of standard deviation.
- It has been demonstrated that the standard deviation estimate is independent of the transmitted symbol and can be obtained from the signal variance estimate.
- An approach in which, in the process of adjusting the equalizer and reducing the dispersion of the output signal, the cost function switches to an algorithm with a large number of detection zones was proposed.
- It was proposed to use a stop-and-go approach to adjust the equalizer in the case of the unidirectional equalization of two algorithms.
- The simulation results showed that the proposed approach provides the adjustment speed of CMA and the residual error level of EDAMA.

5 FPGA IMPLEMENTATION AND FIELD MEASUREMENTS

5.1 Design Objectives

The IP core to be implemented is a linear complex half-baud-spaced blind equalizer. It is realized using the direct form complex equalizer structure, consisting of four real finite impulse response (FIR) filters. The IP core operates twice the symbol frequency and uses two clock-enable signals: one operates twice the symbol frequency, and the other operates at the symbol frequency. The equalizer output and tap coefficients are updated once per symbol period. The equalizer is configurable and capable of working with QAM modulation orders from 4-QAM to 128-QAM. Several debugging functions designed to evaluate the equalizer performance have also been implemented on the VHDL. There are two pipelining stages: the first stage is after the equalizer output is generated, while the second stage follows the error signal calculation. The primary goals of this implementation are:

- to implement an IP core of a dynamic complex equalizer for QAM signals in Matlab and implement this core in VHDL;
- to design the debug constructions that allow the construction of the equalizer's convergence curves in the FPGA and download them;
- to verify a possibility of the designed device to mitigate the multipath propagation effects for QAM modulation of the order from 4-QAM to 128-QAM;
- to connect the blind equalizer IP core to the QAM receiver to test equalization capabilities using physical-world signals.

5.2 Fixed-Point Arithmetic Implementation

The practical implementation of the algorithm in FPGA requires a transition to integer arithmetic. The equalizer input signal was digitized using a 12-bit ADC, then processed while maintaining the bit depth. Empirically, it was found that using 16 bits to represent the value of the coefficients is sufficient to ensure the convergence of the equalizer. Also, with this number of bits, the equalizer does not increase the dispersion of the output signal. In the previous chapters, the expression for updating the coefficients was presented as:

$$c[l, k+1] = c[l, k] - \mu \left(\left| s_{\text{ex}}[k] \right|^2 - R_j^2 \right) s_{\text{ex}}[k] s_{\text{in}}^*[k-l], \tag{5.1}$$

where R_j is dispersion constant for current detection zone.

Expression (5.1) shows that updating the equalizer tap weight depends on the corresponding input sample and common value for all coefficients on a given cycle. Getting this value requires the product of three variables, which increases the word length of the result. Preservation of the

adjustment accuracy with a decrease in the bit width of this value is ensured by switching to floating-point arithmetic with a radix of 2. The value is converted to a fixed-point number using a multiplexer when updating the equalizer tap weight. Note that the step-size coefficient is applied as a power of two without a mantissa to simplify implementation. Updates of the equalizer taps weights are averaged using 32-bit accumulators. The 16 most significant bits of these accumulators are used as equalizer coefficients.

5.3 Blind Equalizer Implementation

It was noted that the practical implementation of the proposed algorithm consists of four real filters with variable dynamic tuning coefficients. Each contains a half-baud-spaced 35-tap delay line and is implemented in direct form using built-in multiply-and-accumulate blocks. The delay line also stores the input signal samples needed to generate the coefficient update. Calculating these values requires performing the steps described in Section 5.2. In practice, a stable implementation requires them to be divided into several clock cycles. Therefore, maintaining the correspondence of the input signal sample and the equalizer tap requires an increase in the length of the filter delay line.

The proposed algorithm offers a cost function that requires detecting the received signal. The boundaries of the detection zones and the dispersion constants of these detection zones are stored in a distributed random access memory. Their use in coefficient update calculation involves a number of multiplexers. Switching between algorithms with a different division of the constellation into detection zones requires an estimate of the output signal dispersion. Averaging, in this case, is performed by a first-order narrow-band low-pass filter with an infinite impulse response. A control node is also implemented that uses hysteresis decision-making to switch between algorithms.

The simulations of the implemented IP core was performed in Xilinx Vivado environment. The results are illustrated for CMA, EDAMA, and generalized algorithm for 10 dB and 15 dB notch channels in Figs 5.1 and 5.2, respectively.

The steady-state performance of the VHDL implemented algorithm is nearly identical to that of the floating-point algorithm for all simulations.

5.4 FPGA Test Environment Implementation

The evaluation of the performance of an equalizer is based on its ability to converge under given conditions. The convergence curves are necessary to draw conclusions about the adequacy of the proposed implementation. Since, in the case of FPGA implementation for 20–40 MHz bands, the equalizer convergence time is measured in tens of microseconds, the curve should be built automatically in FPGA.

To build a convergence curve, an estimate of the variance of the output signal, calculated in the equalizer, is used. After the equalizer exits the reset state, the saving of convergence curve values is

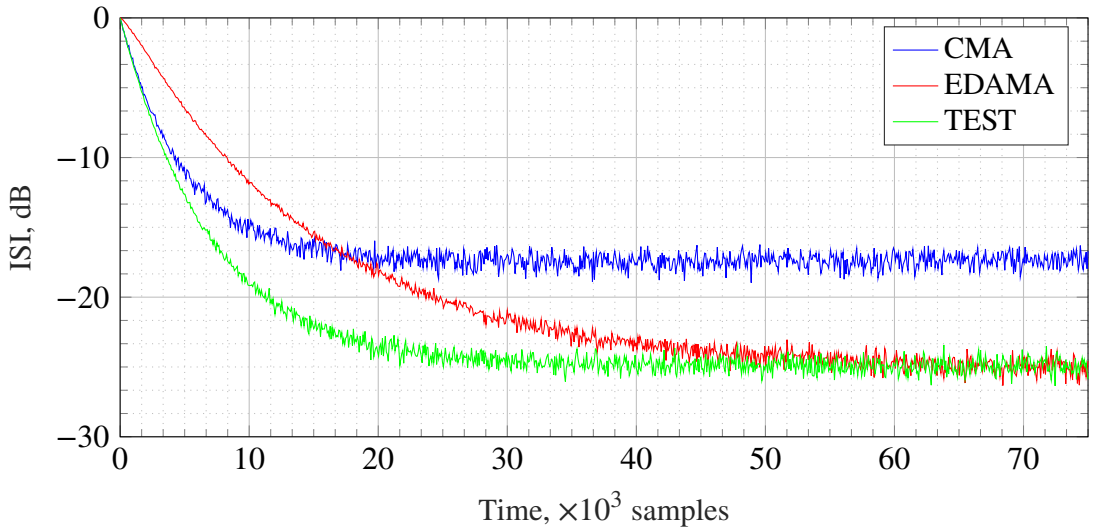

Fig. 5.1. Convergence curves for CMA, EDAMA, and the proposed algorithm in the case of the 10 dB notch channel

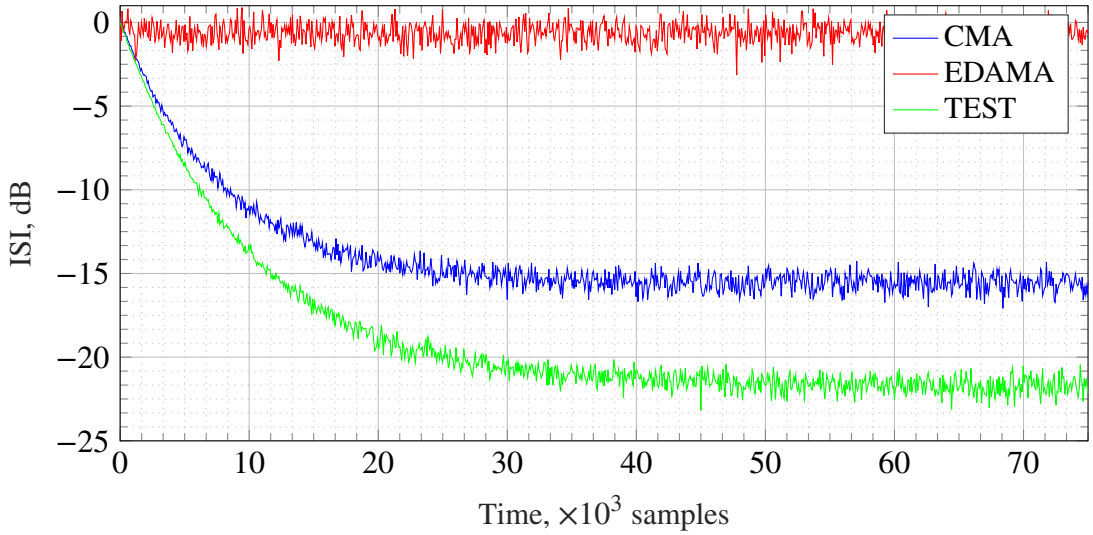

Fig. 5.2. Convergence curves for CMA, EDAMA, and the proposed algorithm in the case of 15 dB noth channel

controlled by a free-running counter. Once every certain number of cycles, the value of the variance estimate is sampled. The intersymbol interference value for the modulation used is estimated based on the dispersion value. The obtained value is afterward written into a memory block. After the equalizer converges, the stored values are read in from the FPGA.

5.5 Implementation Results

Verification of the implemented block took place at several stages of development. First, separating the math involved in updating the equalizer weights into a chain of simple actions and the pipeline resulted in increased latency in the equalizer feedback loop. Secondly, the transition to fixed-point arithmetic can be interpreted as introducing an additional noise component into the values of the

coefficients. Both of these operations were performed in the Matlab environment, after which the simulation was restarted. After that, the finished model was rewritten in the VHDL language. Several single launches were made in the Vivado Simulator with signals synthesized in Matlab fed to the equalizer input to check the bit-to-bit compatibility between the models. The goal, in this case, was to obtain a signal at the output of the equalizer identical to that in the Matlab environment.

After verification, the IP core was synthesized using Xilinx Vivado. The compiled core was incorporated into the QAM modem project. The final device, which is the receiving part of the data transmission system based on QAM, was tested in the field. The ability to converge at initial deep notches was demonstrated on a multipath emulator. Connecting the device to a line of multiple analog repeaters has shown improved performance in the event of band-limiting and system ripples. Inside the FPGA, the equalizer weights were repeatedly reset and the MSE was read at the equalizer output as a function of time. Thus, as a result of averaging, convergence curves were obtained for each of the equalizer algorithms. The resulting convergence curves are shown in Fig. 5.3.

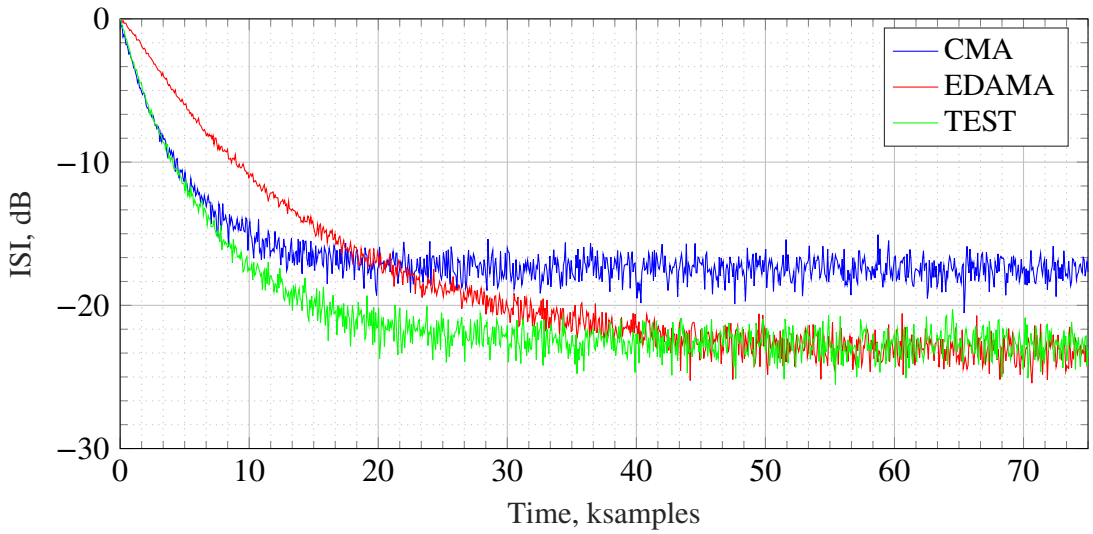

Fig. 5.3. FPGA read convergence curves for CMA, EDAMA and the proposed algorithm in the case of 15 dB notch channel

5.6 Conclusions

This chapter was devoted to the implementation of blind equalization algorithms on VHDL and subsequent verification of their performance in FPGA. In this regard, the following points should be noted.

- The problems of equalization and adjustment of the equalizer coefficients were decomposed into simple mathematical or logical operations to enable their description in VHDL.
- The decomposition of logically related operations into groups was carried out to ensure the possibility of their implementation in a parallel environment.

- The detection implementation was optimized in order to minimize the resources used by the FPGA.
- Rounding and implementation of blocks in integer arithmetic and with a limited word length was made.
- The created IP core was incorporated into the existing QAM modem project, and its performance was verified.

FINAL CONCLUSIONS

This Doctoral Thesis is devoted to the issues of blind equalization of QAM signals. The author has proposed several approaches to forming cost functions for blind equalization algorithms. Practical implementation and field tests of the final device showed the engineering viability of the proposed technique for blind equalization. In particular, the alignment algorithms presented in the Thesis simultaneously provide a high convergence capability under conditions of significant initial multipath distortion. At the same time, these algorithms show a low residual error level in the signal at the output of the equalizer after its adjustment. This feature eliminates the necessity of usual switching to decision-directed channel changes tracking algorithms after converging the equalizer. The practical applicability of the proposed solutions also justifies finding a commercial application of the developed device.

The most important results of the research carried out within the framework of this Doctoral Thesis are as follows.

- The work suggests the optimal calculation of detection thresholds for estimating the received symbol at the output of the equalizer. A combination of methods for calculating thresholds and a CMA-based equalizer adjustment cost function is proposed in [38]. This algorithm makes it possible to reduce the residual error level down to zero in the absence of noise at the equalizer input and its infinite length.
- A probability density was proposed as a metric for assessing the equalizer misadjustment probability at a certain radius of the output. As a solution to reduce misadjustment probability, in [39], it is proposed to merge constellation circles in regions of high misadjustment probability density.
- The Thesis proposes switching between algorithms with different combinations of constellation circles to consider the level of variance in the output signal. The approach was first described in [40] and showed a high convergence capability with a low residual error level.
- Practical implementation and verification showed the characteristics of the proposed algorithms corresponding to the simulations. Some implementation details were published in [37].

Thus, we can conclude that the proposed methodology of QAM signals equalization is practically applicable and that the objective set for this Thesis has been successfully achieved. Moreover, the results obtained can be easily extended to more sophisticated communication schemes that use the QAM concept.

BIBLIOGRAPHY

[1] Y. Sato. "A Method of Self-Recovering Equalization for Multilevel Amplitude-Modulation Systems." In: *IEEE Trans. Commun.* 23.6 (June 1975), pp. 679–682. ISSN: 0096-2244. DOI: 10.1109/TCOM.1975.1092854.

[2] D. N. Godard. "Self-Recovering Equalization and Carrier Tracking in Two-Dimensional Data Communication Systems." In: *IEEE Trans. Commun.* 28.11 (Nov. 1980), pp. 1867–1875. ISSN: 0096-2244. DOI: 10.1109/TCOM.1980.1094608.

[3] W. Sethares, G. Rey, and C. R. Johnson Jr. "Approaches to Blind Equalization of Signals with Multiple Modulus." In: *IEEE International Conference on Acoustics, Speech, and Signal Processing (ICASSP-89)*. Vol. 89. Glasgow, UK: IEEE, May 1989, pp. 972–975. DOI: 10.1109/ICASSP.1989.266592.

[4] M. J. Ready and R. P. Gooch. "Blind Equalization Based on Radius Directed Adaptation." In: *International Conference on Acoustics, Speech, and Signal Processing*. Albuquerque, USA: IEEE, Apr. 1990, pp. 1699–1702. DOI: 10.1109/ICASSP.1990.115806.

[5] K. N. Oh and Y. O. Chin. "Modified Constant Modulus Algorithm: Blind Equalization and Carrier Phase Recovery Algorithm." In: *Gateway to Globalization*. Vol. 1. Seattle, USA: IEEE, June 1995, pp. 498–502. ISBN: 978-0-7803-2486-2. DOI: 10.1109/ICC.1995.525219.

[6] J. Yang, J.-J. Werner, and G. A. Dumont. "The Multimodulus Blind Equalization and Its Generalized Algorithms." In: *IEEE J. Select. Areas Commun.* 20.5 (June 2002), pp. 997–1015.

[7] S. Abrar and R. A. Axford Jr. "Sliced Multi-Modulus Blind Equalization Algorithm." In: *ETRI Journal* 27.3 (June 2005), pp. 257–266. ISSN: 1225-6463. DOI: 10.4218/etrij.05.0104.0027.

[8] V. Weerackody and S. A. Kassam. "Dual-Mode Type Algorithms for Blind Equalization." In: *IEEE Trans. Commun.* 42.1 (Jan. 1994), pp. 22–28.

[9] G. Picchi and G. Prati. "Blind Equalization and Carrier Recovery Using a "Stop-and-Go" Decision-Directed Algorithm." In: *IEEE Trans. Commun.* 35.9 (Sept. 1987), pp. 877–887. ISSN: 0096-2244. DOI: 10.1109/TCOM.1987.1096877.

[10] M. Shahmohammadi and M. Kahaei. "A New Dual-Mode Approach to Blind Equalization of QAM Signals." In: *Eighth IEEE International Symposium on Computers and Communication (ISCC 2003)*. Kemer, Turkey: IEEE, July 2003.

[11] R. A. Axford Jr., L. Milstein, and J. Zeidler. “A Dual-Mode Algorithm for Blind Equalization of QAM Signals: CADAMA.” In: *Conference Record of the Twenty-Ninth Asilomar Conference on Signals, Systems and Computers*. Vol. 1. Pacific Grove, USA: IEEE Comput. Soc. Press, 1996, pp. 172–176. ISBN: 978-1-55937-533-7 978-0-8186-7370-2. DOI: 10.1109/ACSSC.1995.540535.

[12] W. SiYuan. “Blind Equalization of QAM Signals Based On Dual-Mode Multi-modulus Algorithms.” In: *Procedia Engineering* 15 (2011), pp. 2434–2438. ISSN: 18777058. DOI: 10.1016/j.proeng.2011.08.457.

[13] C.-H. Tseng and C.-B. Lin. “A Stop-and-Go Dual-Mode Algorithm for Blind Equalization.” In: *Communications: The Key to Global Prosperity*. Vol. 2. London, UK: IEEE, Nov. 1996, pp. 1427–1431. ISBN: 978-0-7803-3336-9. DOI: 10.1109/GLOCOM.1996.587681.

[14] L. Litwin et al. “Blended CMA: Smooth, Adaptive Transfer from CMA to DD-LMS.” In: *IEEE Wireless Communications and Networking Conference, 1999*. New Orleans, USA: IEEE, 1999, pp. 797–800. ISBN: 978-0-7803-5668-9. DOI: 10.1109/WCNC.1999.796764.

[15] S. Abrar. “Stop-and-Go Algorithms for Blind Channel Equalization in QAM Data Communication Systems.” In: *National Conference on Emerging Technologies*. Pakistan, Dec. 2004.

[16] D. Ashmawy et al. “Joint MCMA and DD Blind Equalization Algorithm with Variable Step-Size.” In: *IEEE International Conference on Electro/Information Technology* (June 2009), pp. 174–177.

[17] Z. Jiang et al. “A Newly High-Speed MCMA Algorithm for QAM System.” In: *4th International Conference on Wireless Communications, Networking and Mobile Computing*. Dalian, China: IEEE, Oct. 2008, pp. 1–4. ISBN: 978-1-4244-2107-7. DOI: 10.1109/WiCom.2008.443.

[18] M. Kaur, P. Singh, and S. Singh. “CMA Technique: A Solution for Minimum PAPR in OFDM.” In: *2nd International Conference on Recent Advances in Engineering & Proceedings of Computational Sciences (RAECS)*. Chandigarh, India: IEEE, Dec. 2015, pp. 1–4. ISBN: 978-1-4673-8253-3. DOI: 10.1109/RAECS.2015.7453323.

[19] R. Mahmoud et al. “A Calibration Method for Hybrid Technique Based on CMA with Clipping in MIMO-OFDM System.” In: *2018 11th German Microwave Conference (GeMiC)*. Freiburg: IEEE, Mar. 2018, pp. 203–206. ISBN: 978-3-9812668-8-7. DOI: 10.23919/GEMIC.2018.8335065.

[20] T. Huang, K. Ren, and X. Li. “Full-Range Carrier Frequency Offset Estimation for CO-OFDM Based on CMA Equalizers.” In: *16th International Conference on Optical Communications and Networks (ICOCN)*. Wuzhen, China: IEEE, Aug. 2017, pp. 1–3. ISBN: 978-1-5386-3271-0 978-1-5386-3273-4. DOI: 10.1109/ICOCN.2017.8121597.

[21] S. Kun and Z. Xudong. “A New CMA-based Blind Equalization for MIMO Systems.” In: *International Conference on Communications, Circuits and Systems (ICCCAS)*. Vol. 1. Chengdu, China: IEEE, 2004, pp. 167–171. ISBN: 978-0-7803-8647-1. DOI: 10.1109/ICCCAS.2004.1345998.

[22] P. O. Taiwo and A. Cole-Rhodes. “MIMO Equalization of 16-QAM Signal Blocks Using an FFT-based Alphabet-Matched CMA.” In: *51st Annual Conference on Information Sciences and Systems (CISS)*. Baltimore, USA: IEEE, Mar. 2017, pp. 1–6. ISBN: 978-1-5090-4780-2. DOI: 10.1109/CISS.2017.7926076.

[23] X. Xiang et al. “Performance Comparison of DA-TDE and CMA for MIMO Equalization in Multimode Multiplexing Systems.” In: *14th International Conference on Optical Communications and Networks (ICOCN)*. Nanjing, China: IEEE, July 2015, pp. 1–3. ISBN: 978-1-4673-7373-9. DOI: 10.1109/ICOCN.2015.7203722.

[24] L. Cui et al. “Research on Cross-Polarization Interference Canceller with Blind Adaptive Algorithm.” In: *International Conference on Computational Problem-Solving (ICCP)*. Leshan, China: IEEE, Oct. 2012, pp. 202–204. ISBN: 978-1-4673-1697-2 978-1-4673-1696-5 978-1-4673-1694-1 978-1-4673-1695-8. DOI: 10.1109/ICCPS.2012.6384214.

[25] M. S. Faruk. “Modified CMA Based Blind Equalization and Carrier-Phase Recovery in PDM-QPSK Coherent Optical Receivers.” In: *16th International Conference on Computer and Information Technology (ICCIT)*. Khulna, Bangladesh: IEEE, Mar. 2014, pp. 469–472. ISBN: 978-1-4799-3497-3 978-1-4799-3496-6. DOI: 10.1109/ICCITechn.2014.6997333.

[26] W. Liu et al. “Two Modified Constant Modulus Methods Based on Independent Component Analysis for Polarization Demultiplexing.” In: *16th International Conference on Optical Communications and Networks (ICOCN)*. Wuzhen, China: IEEE, Aug. 2017, pp. 1–3. ISBN: 978-1-5386-3271-0 978-1-5386-3273-4. DOI: 10.1109/ICOCN.2017.8121523.

[27] K. Sekiyama et al. “Blind Signal Separation Using Array Antenna with Modified Optimal-Stepsize CMA.” In: *2020 International Symposium on Antennas and Propagation (ISAP)*. Osaka, Japan: IEEE, Jan. 2021, pp. 799–800. ISBN: 978-4-88552-326-7. DOI: 10.23919/ISAP47053.2021.9391234.

[28] J. Tagapanij et al. “Phased Array of Switched-Beam Elements for Handset Adaptive Antenna.” In: *2007 IEEE Radio and Wireless Symposium*. Long Beach, CA, USA: IEEE, 2007, pp. 137–140. ISBN: 978-1-4244-0444-5. DOI: 10.1109/RWS.2007.351786.

[29] M. Krairiksh. “Development of a Handset Adaptive Antenna Using Phased-Array of Switched-Beam Elements.” In: *2008 International Workshop on Antenna Technology: Small Antennas and Novel Metamaterials*. Chiba, JApan: IEEE, Mar. 2008, pp. 87–90. ISBN: 978-1-4244-1522-9. DOI: 10.1109/IWAT.2008.4511297.

[30] K. Maruta and C.-J. Ahn. “Enhanced Semi-Blind Uplink Interference Suppression on Multicell Massive MIMO Systems for Multi Modulus Signals.” In: *2019 IEEE 90th Vehicular Technology Conference (VTC2019-Fall)*. Honolulu, HI, USA: IEEE, Sept. 2019, pp. 1–6. ISBN: 978-1-72811-220-6. DOI: 10.1109/VTCFall.2019.8891412.

[31] K. Maruta and C.-J. Ahn. “Uplink Interference Suppression by Semi-Blind Adaptive Array With Decision Feedback Channel Estimation on Multicell Massive MIMO Systems.” In: *IEEE Trans. Commun.* 66.12 (Dec. 2018), pp. 6123–6134. ISSN: 0090-6778, 1558-0857. DOI: 10.1109/TCOMM.2018.2863679.

[32] B. Yang, D. Wang, and Y. Wu. “Joint Batch Implementation of Blind Equalization and Timing Recovery.” In: *Journal of Communications* 8.7 (2013), pp. 449–455. ISSN: 17962021. DOI: 10.12720/jcm.8.7.449-455.

[33] M. S. Faruk. “Low Complexity Carrier-Phase Estimation Based on Sign-Error Modified CMA for 16-QAM Coherent Optical Receivers.” In: *3rd International Conference on Electrical Information and Communication Technology (EICT), 2017*. Khulna, Bangladesh: IEEE, Dec. 2017, pp. 1–3. ISBN: 978-1-5386-2305-3 978-1-5386-2307-7. DOI: 10.1109/EICT.2017.8275194.

[34] D. Kolosovs and E. Bekeris. “Chaos Code Division Multiplexing Communication System.” In: *7th International Conference on Computational Intelligence, Communication Systems and Networks (CICSyN)*. Riga, Latvia: IEEE, June 2015, pp. 65–69. ISBN: 978-1-4673-7016-5. DOI: 10.1109/CICSyN.2015.22.

[35] F. Capligins et al. “FPGA Implementation and Study of Synchronization of Modified Chua’s Circuit-Based Chaotic Oscillator for High-Speed Secure Communications.” In: *2020 IEEE 8th Workshop on Advances in Information, Electronic and Electrical Engineering (AIEEE)*. Vilnius, Lithuania: IEEE, Apr. 2021, pp. 1–6. ISBN: 978-1-66542-538-4. DOI: 10.1109/AIEEE51419.2021.9435783.

[36] F. Capligins, A. Litvinenko, and D. Kolosovs. “FPGA Implementation and Study of Antipodal Chaos Shift Keying Communication System.” In: *2021 IEEE Microwave Theory and Techniques in Wireless Communications (MTTW)*. Riga, Latvia: IEEE, Oct. 2021, pp. 1–6. ISBN: 978-1-66542-469-1. DOI: 10.1109/MTTW53539.2021.9607226.

[37] S. Šarkovskis et al. “Encoder Improvement for Simple Amplitude Fully Parallel Classifiers Based on Grey Codes.” In: *Procedia Engineering* 178 (2017), pp. 604–614. ISSN: 18777058. DOI: 10.1016/j.proeng.2017.01.119.

[38] D. Kolosovs, A. Zelenkov, and A. Jersovs. “Enhanced Decision Adjusted Modulus Algorithm for Blind Equalization.” In: *Procedia Computer Science* 104 (2017), pp. 429–436. ISSN: 18770509. DOI: 10.1016/j.procs.2017.01.156.

[39] D. Kolosovs. “A Generalization of the Enhanced Decision Adjusted Modulus Algorithm for Blind Equalization of Constellations with Closely Positioned Circles.” In: *2020 IEEE Microwave Theory and Techniques in Wireless Communications (MTTW) (MTTW’20)*. Riga, Latvia: IEEE, Oct. 2020, pp. 195–200. ISBN: 978-1-72819-398-4. DOI: 10.1109/MTTW51045.2020.9244924.

[40] D. Kolosovs. “A Multi-Mode Approach for the Enhanced Decision Adjusted Modulus Algorithm Usage in Blind Equalization of QAM Signals.” In: *2021 IEEE Microwave Theory and Techniques in Wireless Communications (MTTW)*. Riga, Latvia: IEEE, Oct. 2021, pp. 40–45. ISBN: 978-1-66542-469-1. DOI: 10.1109/MTTW53539.2021.9607265.

[41] P. Bello. “Characterization of Randomly Time-Variant Linear Channels.” In: *IEEE Trans. Commun.* 11.4 (Dec. 1963), pp. 360–393. ISSN: 0096-2244. DOI: 10.1109/TCOM.1963.1088793.

[42] B. Molnar et al. “The WSSUS Channel Model: Comments and a Generalisation.” In: *Proceedings of GLOBECOM’96. 1996 IEEE Global Telecommunications Conference*. London, UK: IEEE, 1996, pp. 158–162. ISBN: 978-0-7803-3336-9. DOI: 10.1109/GLOCOM.1996.586800.

[43] M. C. Jeruchim, P. Balaban, and K. S. Shanmugan, eds. *Simulation of Communication Systems: Modeling, Methodology, and Techniques*. 2nd ed. Information Technology–Transmission, Processing, and Storage. New York: Kluwer Academic/Plenum Publishers, 2000. ISBN: 978-0-306-46267-2.

Deniss Kolosovs was born in 1990 in Riga. He obtained a Bachelor's degree in Electronics in 2012 and a Master's degree in Electronics in 2014 from Riga Technical University. He has been an engineer in JSC "SAF Tehnika" since 2014. Currently, he is a lecturer at Riga Technical University. His research interests include signal processing, digital telecommunications systems, and adaptive filters.